To cite this version :

Ibrahim GODA, Jérémie GIRARDOT - A computational framework for energy absorption and damage assessment of laminated composites under ballistic impact and new insights into target parameters - Aerospace Science and Technology - Vol. 115, p.106835 - 2021

A computational framework for energy absorption and damage assessment of laminated composites under ballistic impact and new insights into target parameters

Ibrahim Goda *, Jérémie Girardot

Arts et Metiers Institute of Technology, University of Bordeaux, CNRS, Bordeaux INP, INRAE, HESAM Université, I2M Bordeaux, F-33400 Talence, France

ABSTRACT

In this research, by means of advanced methods within the framework of the FE method, an effective modeling approach is proposed to simulate the ballistic perforation behaviors of multi-directional woven composite panels. Within that scope, constitutive models for intraply and interfacial or interply damage mechanisms are formulated and implemented into ABAQUS/Explicit FE code. The constitutive law of ply-level damage model incorporates the nonlinear material response, degradation of material properties, progressive failure and the element deletion scheme. The interfaces between the individual plies are modeled using a cohesive surface method, and the behaviors of interply degradation and failure are described using a traction-separation law. Besides, the material responses with large nonlinearity due to fiber rupture, matrix cracking, plasticity effects due to micro-matrix cracking under shear loading, and interface delamination are accounted for by appropriate material degradation models. The proposed developments are first validated against the available experimental and analytical results. Next, the ballistic impact simulations of woven composite targets are carried out in a two-phase research. The first phase analyzes the ballistic impact behavior and ballistic performance of the composite laminates in terms of residual velocity and energy absorbing capacity. The second phase involves the investigation of the impact characteristics and failure mechanisms of the composite materials. More specifically, the key perforation mechanisms and associated impact damage extents and patterns with respect to projectile velocity are investigated for the composite panels. We further perform parametric analysis in order to understand the influence of a certain number of parameters on the laminate ballistic impact response. These parameters are categorized based on materials such as fiber type material, interface systems, and geometry such as stacking sequences and support conditions. Numerical results reveal that the ballistic impact performance depends significantly on the cohesive material properties, the stacking sequence, and the woven fabric material, whereas less contribution of support conditions to the ballistic perforation characteristic is noticed.

1. Introduction

Composite materials have emerged as one of the materials that possess various superiorities such as high specific stiffness and strength properties as well as design flexibility. For such reasons, they have gradually replaced classical metallic materials and have been applied in a variety of commercial and military applications such as automotive, marine and aerospace engineering [1–3]. However, their vulnerability against impact, which is the most unfavorable characteristic of the composite material, poses a threat to the residual load carrying capacity of the composite.

Corresponding author.

E-mail address: ibrahim.goda02@gamil.com (I. Goda).

In a variety of situations, the laminated composite structures are more likely to encounter impact by foreign objects in service life. Understanding the behavior of these composite structures when subjected to localized impact is an important and highly complex problem, and the degree of complexity grows with the increase of the impact velocity [4]. This is principally attributable to the dependency of a variety of factors such as damage mechanisms, material behaviors, and load transfer mechanisms, which are typically complex and conjoined with various uncertainties. As a consequence of this, predicting the impact process leads to an open problem, where investigations have been performed in a number of ways, varying from simple empirical models to highly sophisticated numerical approaches relying on the importance and severity of the impact.

In spite of years of extensive research on impact, a complete and validated methodology for predicting the damage behavior of laminated composite materials has not yet been fully attained [5]. This is mostly due to the complexity of the physical phenomena involved in the impact process, including composite-projectile contact, employed composite damage model, failure modes development and ply-ply interaction within the laminate, influence of velocity, laminate geometry, constraint conditions, and lamination scheme. With special regard to the possible damage occurring in impacted laminates, typical damage reported in the literature consists of a combination of (i) intralaminar damage mechanisms such as fiber damage, matrix cracking or plasticity, and fiber/matrix debonding, and (ii) interlaminar failure, which develops at the interface between adjacent plies in the form of debonding between laminae (delamination) [6,7].

On the basis of energy transfer between the impactor and composite laminate target, energy dissipation and damage propagation mechanisms, the impact load with regard to velocity can be widely classified into four categories including low-velocity, high-velocity, ballistic-velocity, and hyper-velocity impacts [8]. According to the literature, the impact events can generally be simplified by grouping them into two distinct situations, namely, low-velocity impact by a large mass and high-velocity impact by a small mass. After a thoroughgoing literature review, it is revealed that the most of published works on impact of polymer composite materials are concerned with low velocity impact events with relatively high masses and low impact velocities involved [9–27]. Oppositely, there are less works on the high-velocity impact behavior of composites, involving relatively small masses and high impact velocities, e.g. [28–32]. The high velocity impact loads from scenarios like runway debris impact and hail impact are indeed more critical aspects for most composite structures in aeronautics.

The study of high-velocity impact loads is of utmost paramount in the aerospace industry especially when human lives are involved, in order to develop safer structures with the aim of avoiding losses of human and material resources. In terms of aircrafts safety during the take-off, flight and landing phases, damage caused by impact events has become an increasingly serious and disastrous issue. Bird strikes, runway debris and ice/hailstones are examples of impact with high probably of occurrence, which may cause severe damage to aircraft structures, leading sometimes to perforations [33,34]. The Concorde accident in 2000 is an illustrative example in which a tire fragment left in runway impacted the fuel tank on the wing of the aircraft, leading to a catastrophic accident [35]. It has been identified as one of the most important factors in aircraft vulnerability because it can cause numerous structural damage and catastrophic failure. The most recent example of the bird strike problem is the Airbus A321 of the Russian Ural Airlines on 15 August 2019, which the birds collided with during take-off, and thus its dual engines failed [36]. Federal Aviation Administration (FAA), European Aviation Safety Agency (EASA) and Civil Aviation Administration of China (CAAC) have defined the requirements of bird-strike for aircraft structures in their own airworthiness regulations [37].

In certain situations, structural materials are required to display substantial impact resistance to high velocity impact, since this is an essential necessity during ballistic impact. Ballistic impact is commonly referred to as a low-mass, high-velocity impact caused by a propelling source or a projectile onto a target. The composites employed in the design of structures such as aircrafts, defense vehicles, and protective armors against the penetration by high velocity projectiles are of great importance. The quantification and simulation of the high-velocity impact response of these composites is crucial for those who are seeking to improve composite structures for military and aerospace applications. In the present research, we aim at studying the impact resistance of the multilayered composite panels against the ballistic impact. This is important in order to understand how a projectile penetrates into the composite panels at ballistic velocities. In such cases, the ballistic impact of the composites is described as an impact which results in the laminate being completely penetrated. For ballistic velocity impact, specifically for the range of impact considered in the present study, where the projectile penetrates the laminate completely and exits with a residual velocity, the numbers of reported studies are few. To the best of our knowledge, a few studies are available in literature on a fully penetrated impact process of the laminated composite panels through analytical models, experiments and numerical simulations (e.g., [38–47]). Naik and Doshi [38] presented an analytical formulation for the prediction of ballistic impact behavior of thick composites. The formulation was based on wave theory and energy balance between the projectile and the target. Naik and Shrirao [39] exposed an analytical model for the ballistic impact analysis of typical plain weave E-glass/epoxy and twill weave T300 carbon/epoxy composites. This method was based on dynamic mechanical and fracture properties of the composite materials, geometrical parameters of the composite target and the projectile parameters, such as mass, velocity, shape and size. Wen [40,41] developed analytical equations to investigate the penetration and perforation of fiber-reinforced plastic laminates by rigid projectiles with different nose shapes. The models were based on the assumption that deformations during a ballistic impact event are localized and the mean pressure offered by the laminate to resist the projectile consists of both cohesive quasi-static resistive pressure due to elastic-plastic deformation and dynamic resistive pressure due to velocity effects. Naik et al. [42,43] carried out analytical and experimental studies on ballistic impact behavior of woven fabric composite laminates against flat projectiles. The work describes energy absorption by different mechanisms, ballistic limit, contact duration, damage size and effect of projectile and target parameters on energy absorption. Yen [44] developed a ply-level material constitutive model for plain-weave composite laminates to enable computational analyses of progressive damage/failure in the laminates under high velocity ballistic impact condition. The model was implemented within LS-DYNA as a user-defined material subroutine to predict the damage and ballistic behavior of composite laminates subjected to various ballistic impact conditions. Reddy et al. [45] performed experimental studies to describe the ballistic performance of E-glass/phenolic laminates impacted at different velocities by mild steel core projectile. The effect of thickness and velocity on energy absorption in the laminates has been explained in terms of interaction time between target and projectile. Karahan et al. [46] investigated experimentally the fiber type, fabric structure, orientation of fabric plies and thickness on the ballistic impact performance of aramid and ultra-high molecular weight polyethylene composite laminates. Patel et al. [47] developed a damage model using FE code to simulate the post impact progressive damage of the composite beams under ballistic impact. The uncertainty in the elastic properties and strength of the composite material were considered in the damage analysis. The ply arrangements for optimum design of simply supported boundary conditions were also discussed.

Respecting the dynamic investigations of composites, much attention has shifted from experimental lab work to numerical simulation because of the high costs of physical testing and the incapacity to precisely monitor the damage states, particularly for high velocity impacts that can induce damage that is nearly undetectable. Among the developed numerical approaches, the progressive damage models have become the most prevalent simulation scheme that accounts for initial damage criteria and subsequent stiffness degradation. Nevertheless, the effects of various failure criteria and damage accumulation laws on high velocity impact predictions for composite materials have not so far been consis-
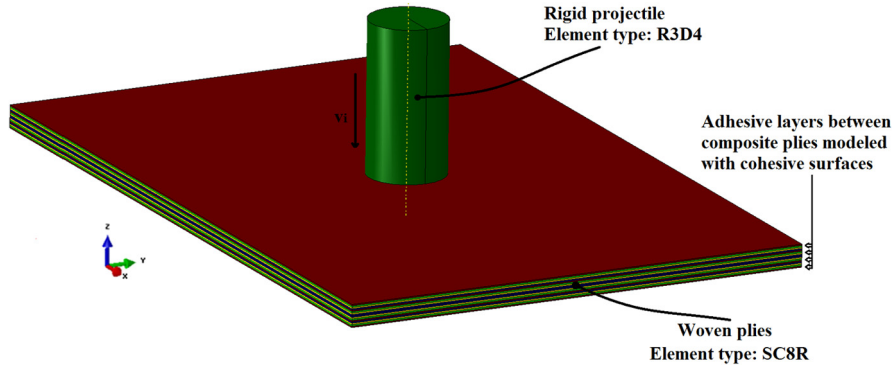
Fig. 1. Schematic illustration of the 3D geometrical model used for ballistic impact simulations.

tently investigated and require further exploration. In this context, a nonlinear dynamic finite element simulation with progressive damage mechanics model is presently developed to systematically explore the ballistic perforation behaviors of woven-fabric reinforced polymer (WFRP) composites when impacted with high velocity projectiles. For such analysis, the explicit simulations of the ballistic impacts often utilize cohesive element formulations to capture the interlaminar behavior. These cohesive elements are computationally expensive because they are frequently the primary driver in the critical time step calculation. Surface-based cohesive zone formulations promise a less severe effect on the overall simulation computational effort [48]. To develop numerical approaches which capture the effects in ballistic impact with the help of surface based cohesive formulations is one of the main goals of this research.

Thus, the scope of the present paper is to use progressive failure models based on continuum damage mechanics in combination with cohesive surface interaction method for modeling structural response and failure mechanisms of woven composite targets subjected to ballistic velocity impact. The constitutive law for composite damage model is formulated and implemented into the FE code ABAQUS/Explicit through VUMAT user subroutine. It incorporates nonlinear material response, degradation of material properties, progressive failure and element deletion scheme. First, the validity of the developed FE model is assessed by available experimental and analytical results in the literature. Then, through the numerical analysis of the proposed models, significant insights into perforation resistance, energy dissipation and damage propagation mechanisms are gained.

Motivated by this framework, the basic objective of the performed ballistic impact simulations in the current work is twofold. First, to assess the capability of simulation approaches based on the combined use of cohesive surface models for progressive interface delamination (shape and extent of individual delaminations at different interfaces) and continuum ply damage models to properly capture the detailed through-thickness distribution of damage induced by ballistic impact in composite laminates. Second, to evaluate the energy dissipation corresponding to different failure modes such as dissipated energy due to the intraply damage, the interply or interface failure, laminate's kinetic energy and the friction dissipation. What's more, a comprehensive parametric study is carried out to further understand the influence of a certain number of parameters on the target ballistic impact behaviors. The parameters studied can be grouped into two key types that are material-based parameters and include the type of fabric materials and interface systems, and geometry-based parameters such as stacking sequence and boundary conditions.

2. Ballistic impact modeling strategy

Ballistic impact of fabric reinforced laminates, in general, is a highly dynamic loading scenario involving nonlinear material behavior. In this section, the FE method is employed to model the laminated composites in a ballistic impact scenario. The modeling scheme is accomplished within the context of the FE method, wherein an explicit time integration scheme is used. The FE models are established for the projectile and composite laminae in FE Abaqus/Explicit. To study the ballistic impact situation between the projectile and the laminate, geometrical modeling, constitutive relations, contact behavior modeling and boundary conditions with relevant analysis procedures are discussed. The constitutive theories including such failure mechanisms as intraply and interply fracture behaviors for composite laminae are systematically taken into consideration. The acting mechanisms can be classified by their location of occurrence into intraply and interply. The mechanisms associated with intraply damage involve fiber rupture and matrix micro-cracking considering plasticity in the plies whereas interply failure signifies the decohesion of adjacent laminae which is commonly referred as delamination. Both of these mechanisms do contribute to the laminate's overall response and their interaction leads to laminate penetration or perforation according to the specified impact scenario. Consequently, the proposed modeling strategy has the potential to describe the key perforation mechanisms and impact-induced damage patterns as well as predicting the overall energy absorption of the laminate and energy contributions of individual mechanisms.

2.1. Geometrical modeling and boundary conditions

The FE model consists of two distinct parts: projectile and composite laminate. The projectile has a cylindrical blunt shape, that is widely used in the literature [42,43,49–52] as it can produce a wide range of failure mechanisms and thus allows a better understanding of the penetration phenomena. The deformation of the projectile is neglected and modeled as a rigid body with the discrete rigid element (R3D4). This is justified by experimental observations with a high-speed camera and damage morphology analysis, see [50]. On the other side, the composite laminate composed of many layers of fabric plies is modeled as a stack of several homogeneous orthotropic plies connected via interply interfaces. A schematic diagram reflecting the physical condition of the FE model is illustrated in Fig. 1. The sizes of simulated targets and projectiles are specified in each relevant section. Utilizing the continuum shell elements, the plies are discretized by a regular mesh of eight-noded, reduced integrated, linearly interpolated continuum shell elements, type SC8R. The mesh size of 1 mm by 1 mm with one through-the-thickness element per ply is found

to achieve a good compromise between accuracy and computational efficiency. The employed continuum based shell elements are similar to 3D continuum solid elements, but their kinematic and constitutive behaviors are based on a shell theory. They are computationally more efficient when compared to solid elements and are typically able to accurately capture the bending deformation caused by the impact [53,54]. In constructing the composite laminate, it shall be noted that the laminate is modeled as a stack of layers connected by zero-thickness interfaces; this is a more physical approach which is closed to the real build up lamination. Indeed, this strategy is much complicated, mainly due to the fact that the preparation of the model is not automatic and shall be performed manually. However it does provide an accurate representation of the laminate layup particularly with regard to contact interactions.

Unless otherwise indicated, the four edges of the laminated target are fully fixed to prevent rigid motion during the impact and the projectile movement is also fixed for all degrees of freedom except for translation along z-direction so as to impose impact velocity.

2.2. Constitutive modeling

Ply-level and interface materials constitutive models are used here for computational analysis of progressive damage/failure in fabric laminates under ballistic impact condition. At the ply-scale, the mechanisms associated with intraply failure are accounted for by an energy based continuum damage mechanics approach to model tensile and compressive damage along the fiber directions. Besides, under shear loading, the plastic deformation and damage are modeled for the purpose of capturing the shear response that is dominated by the matrix of the ply.

For the considered woven fabric-reinforced plies, the fiber directions are assumed to be orthogonal. Therefore, the constitutive elastic stress-strain relations coupled to damage in a local coordinate system with the base vectors aligned with fiber directions are as follows [55]:

$$
\underbrace{\left\{\begin{array}{c} \varepsilon_{11} \\ \varepsilon_{22} \\ \varepsilon_{12}^e \end{array}\right\}}_{\varepsilon} \left[\begin{array}{ccc} \frac{1}{(1-d_1)E_1} & \frac{-\nu_{12}}{E_1} & 0 \\ \frac{-\nu_{21}}{E_2} & \frac{1}{(1-d_2)E_2} & 0 \\ 0 & 0 & \frac{1}{(1-d_{12})2G_{12}} \end{array}\right] \underbrace{\left\{\begin{array}{c} \sigma_{11} \\ \sigma_{22} \\ \sigma_{12} \end{array}\right\}}_{\sigma} \quad (1)
$$

where $\varepsilon_{11}, \varepsilon_{22}, \varepsilon_{12}^e$ and $\sigma_{11}, \sigma_{22}, \sigma_{12}$ are the elastic strains and stresses, respectively. E_1 and E_2 are the Young's moduli along fiber directions 1 and 2, respectively, ν_{12} and ν_{21} are the Poisson's ratios, and G_{12} is the in-plane shear modulus. d_1 and d_2 are damage variables associated with the fiber fracture along the fiber directions, and d_{12} is the damage variable associated with the matrix damage due to the shear deformation. The damage variables fall within the range between 0 (undamaged) and 1 (fully damaged); they depict the degradation in the material caused by different loading conditions.

To distinguish between the tensile and compressive fiber failure modes, the respective damage variables are calculated in conformity with the stress state in the fiber directions 1 and 2 as

$$
d_i = d_{i+} \frac{\langle\sigma_{ii}\rangle}{|\sigma_{ii}|} + d_{i-} \frac{\langle-\sigma_{ii}\rangle}{|\sigma_{ii}|} \quad (2)
$$

where d_{i+} and d_{i-} refer to the tensile $(+)$ and compressive $(-)$ damage variables of the fibers in the ith directions $(i = 1, 2)$, respectively. The damage variables are assumed to evolve as a function of the corresponding effective (undamaged) stress as

$$
d_{i+} = d_{i+}(\tilde{\sigma}_{i+}), d_{i-} = d_{i-}(\tilde{\sigma}_{i-}), d_{12} = d_{12}(\tilde{\sigma}_{12}) \quad (3)
$$

The effective tensile $\tilde{\sigma}_{i+}$, compressive $\tilde{\sigma}_{i-}$, and shear $\tilde{\sigma}_{12}$ stresses given in (3) are formulated as

$$
\tilde{\sigma}_{i+} = \frac{\langle\sigma_{ii}\rangle}{(1-d_{i+})}, \qquad \tilde{\sigma}_{i-} = \frac{\langle-\sigma_{ii}\rangle}{(1-d_{i-})},
$$
$$
\tilde{\sigma}_{12} = \frac{\sigma_{12}}{(1-d_{12})} = 2G_{12}\varepsilon_{12}^e = 2G_{12}(\varepsilon_{12} - \varepsilon_{12}^p) \quad (4)
$$

The damage state is characterized by the loading functions ϕ_{i+}, ϕ_{i-}, ϕ_{12} $(i = 1, 2)$ for different failure mechanisms (fiber failure, matrix cracking and plastic deformation under shear loading), they are expressed as

$$
\phi_{i+} = \frac{\tilde{\sigma}_{i+}}{X_{i+}}, \qquad \phi_{i-} = \frac{\tilde{\sigma}_{i-}}{X_{i-}}, \qquad \phi_{12} = \frac{\tilde{\sigma}_{12}}{S_{12}} \quad (5)
$$

These functions provide five criteria to describe the initiation of fiber failure in directions 1 and 2, and initiation of matrix damage. In eq. (5), X_{i+} and X_{i-} stand for the tensile and compressive strengths for uniaxial loading in each fiber direction, respectively, and S_{12} represents the shear stress required for matrix damage initiation. When the initiation function ϕ_{i+}, ϕ_{i-} or ϕ_{12} is equal to unity, the corresponding damage mode will be activated.

Once the damage initiation criterion is met, the evolution of damage begins, and the above-mentioned damage variables ($d_{i\pm}$, d_{12}) exercise a significant influence on the degradation process of the integration point. The calculation method for addressing the evolution of damage variables d_{i+}, d_{i-}, d_{12} is implemented according to [56,57] by the following expressions

$$
d_{i+} = 1 - \frac{1}{\lambda_{i+}} \exp\left[\frac{-2g_0^{i+} L_c}{G_f^{i+} - g_0^{i+} L_c}(\lambda_{i+} - 1) \right],
$$
$$
d_{i-} = 1 - \frac{1}{\lambda_{i-}} \exp\left[\frac{-2g_0^{i-} L_c}{G_f^{i-} - g_0^{i-} L_c}(\lambda_{i-} - 1) \right] \quad (6)
$$
$$
d_{12} = \min(\alpha_{12} \ln(\lambda_{12}), d_{12}^{\max})
$$

with g_0^i the elastic strain energy density at the point of damage initiation expressed as $g_0^i = X_i^2/2E_i$, L_c the characteristic length of the element, $G_f^{i\pm}$ the fracture energy per unit area under uniaxial tensile and compressive loadings, $\alpha_{12} > 0$ the shear damage parameter, and $d_{12}^{\max} \leq 1$ the maximum shear damage. λ_{i+}, λ_{i-} and λ_{12} in eq. (6) stand for the tensile, compressive, and shear damage thresholds, respectively. They are initially set to one and after damage initiation i.e., $\phi_{i\pm} = 1$, $\phi_{12} = 1$, they increase with damage progression according to $\lambda_{i\pm}(t) = \max_{\tau \leq t} \phi_{i\pm}(\tau)$, $\lambda_{12}(t) = \max_{\tau \leq t} \phi_{12}(\tau)$. After the threshold is reached, the damage happens consequently until the damage variables reach unity to completely fail.

In terms of shear damage, the in-plane shear response is predominated by the nonlinear behavior of the matrix that exhibits both stiffness degradation due to matrix microcracking and plastic deformation. Upon unloading the shear, this results in permanent deformations in the fabric ply. To account for the subsequent inelastic behaviors before complete failure, the classical plasticity model with an elastic domain function and hardening law for the damaged materials are adopted; they are expressed respectively as

$$
F = |\tilde{\sigma}_{12}| - \tilde{\sigma}_0(\bar{\varepsilon}^p) \leq 0 \quad (7)
$$

and

$$
\tilde{\sigma}_0(\bar{\varepsilon}^p) = \tilde{\sigma}_{y0} + C(\bar{\varepsilon}^p)^\gamma \quad (8)
$$

with $\tilde{\sigma}_{y0}$ the initial effective shear yield stress, C and γ the hardening parameters, and $\bar{\varepsilon}^p$ the equivalent plastic strain due to shear deformation.

In the calculation process, the failed continuum shell elements are removed from the model to prevent excessive distortion of the elements which may terminate the calculation and influence the final results. In this work, the damage-based element deletion criterion is employed to eliminate the fully damaged elements. It is activated when any one tensile/compressive damage variable along the fiber directions 1 and 2 reaches a maximum specified value, d_1 or $d_2 = d_{\max} = 1$.

In order to account for the adhesive bonds between adjacent fabric plies and modeling the interply delamination phenomenon, the constitutive laws of surface-based cohesive zone method (CZM) are adopted. Compared to the surface-based method, there is also a cohesive element method, whose use significantly increases the computational complexity of the model as the cohesive element formulation requires a fine mesh which negatively affects the critical time step. Consequently, the surface-based contact approach that follows a similar constitutive behavior as cohesive element is presently used to describe the adhesive interface between the composite plies. The basis of this method is the cohesive behavior interaction of two adjacent surfaces, in which the contact between adhesive surfaces is defined as a surface interaction property with a zero interface thickness. The degradation and fracture for the interfaces are predicted using an uncoupled traction-separation based constitutive law. The two main ingredients of the underlying damage law are damage initiation criterion and damage evaluation law.

Before damage initiation, the mechanical behavior of the interface is assumed to be linear with high values of initial interface stiffness (K_i); it is described by the following constitutive relation that relates the traction stress vector (t_i) to the separation displacements (δ_i) across the interface

$$t = \begin{bmatrix} t_n \\ t_s \\ t_t \end{bmatrix} = \begin{bmatrix} K_n & 0 & 0 \\ 0 & K_s & 0 \\ 0 & 0 & K_t \end{bmatrix} \begin{bmatrix} \delta_n \\ \delta_s \\ \delta_t \end{bmatrix} \tag{9}$$

Firstly, damage onset at the interfaces is predicted using the quadratic nominal stress criterion according to which damage is assumed to be initiated when the quadratic interaction function involving the stress ratios reaches 1. This criterion is expressed as

$$\left(\frac{\langle t_n \rangle}{t_n^{\max}} \right)^2 + \left(\frac{t_s}{t_s^{\max}} \right)^2 + \left(\frac{t_t}{t_t^{\max}} \right)^2 = 1 \tag{10}$$

with t_i and $t_i^{\max}$ ($i = n, s, t$), respectively, the nominal traction stresses and the corresponding interface strengths in the normal n and shear s and t directions.

Secondly, the damage evolution process that describes the degradation of the cohesive stiffness after damage initiation is defined based on the energy that is dissipated as a result of the damage process. An exponential softening law is used to model the evolution of the damage variable from damage initiation to eventual failure. In accordance with the Benzeggagh-Kenane (BK) law, the mixed-mode energy behavior is used to model the progression of damage at the interfaces and takes the following form

$$G_n^C + \left(G_s^C - G_n^C \right) \left(\frac{G_S}{G_T} \right)^{\eta} = G^C \tag{11}$$

with $G_S = G_s + G_t$, $G_T = G_n + G_S$, and the quantities G_n, G_s, and G_t stand for the current fracture toughness in the normal, first, and second shear directions, respectively; G_n^C, G_s^C and G_t^C refer to the corresponding fracture toughness in the normal, first, and second shear directions, respectively. G^C represents the total critical mixed-mode fracture energy and η is a cohesive property coefficient.

In Fig. 2, we illustrate a flowchart of the algorithm for the numerical procedure used to implement the proposed damage models to simulate the ballistic impact of composite laminates, according to which the mechanisms associated with interply failure, i.e. debonding of adjacent plies and intraply damage are accounted for.

2.3. Contact modeling

Given the underlying ballistic impact problem, the loads are applied by a projectile that comes into contact with the laminated plate. Thus, modeling the contact behavior is of great importance for predicting the ballistic impact response. A general contact algorithm available in ABAQUS/Explicit is employed to model the interactions between the debonded woven plies and between the woven plies and the projectile so that the element penetration can be prevented. The contact constraints within the simulation are implemented using the penalty and hard contact formulations. After interface debonding between the adjacent plies takes place, the general contact definition is systematically updated to take into account for possible post-debonding contact. Besides, because the contact surfaces normally transmit shear or normal forces, prescribing a friction contact that describes the force resisting the relative tangential motion of the contact surfaces at integrated points is necessary. In this work, the friction coefficient between the composite laminate and the projectile, and between the surfaces of the debonded fabric layers is set to 0.3. This value is chosen according to the studies available in the literature [58,59].

3. Energy balance of ballistic impact model

The kinetic energy of the projectile plays an important role in the ballistic impact process in the initial stage until reaching the contact instant and it is dissipated into the entire system with different energy forms once the contact occurs. The mechanisms of ballistic impact energy dissipation into the composite laminate system are used to express the energy balance relationship. The energy balance between the kinetic energy of the projectile and the energy absorbed by the various mechanisms is thus expressed as follows

$$\frac{1}{2} m_p V_i^2 = \frac{1}{2} m_p V_r^2(t) + E_{AB}(t) \tag{12}$$

where V_i is the projectile initial (impact) velocity, m_p is the mass of projectile, $1/2 m_p V_i^2$ is the initial (impact) energy, $V_r(t)$ is the projectile residual velocity at time instant t, and $1/2 m_p V_r^2(t)$ represents the residual energy of projectile after impact (E_{RK}). The total absorbed energy at any time during the impact process ($E_{AB}(t)$) can be calculated by

$$E_{AB}(t) = E_{PK}(t) + E_I(t) + E_{VD}(t) + E_{FD}(t) - E_{PW}(t) \tag{13}$$

where E_{PK} is the kinetic energy of composite panels, E_I is the total internal energy, E_{VD} is the viscous dissipation, E_{FD} is the frictional dissipation and E_{pw} is the work done by contact and constraint penalties. The internal energy of the system (E_I) can further be composed of the following terms

$$E_I(t) = E_S(t) + E_A(t) + E_{PD}(t) + E_{DD}(t) \tag{14}$$

with E_S the elastic or recoverable strain energy, E_A the artificial strain energy, E_{PD} the energy dissipated by inelastic process like that of plastic deformation or extensive cracking and E_{DD} the energy dissipated by delamination. The artificial strain energy (E_A),
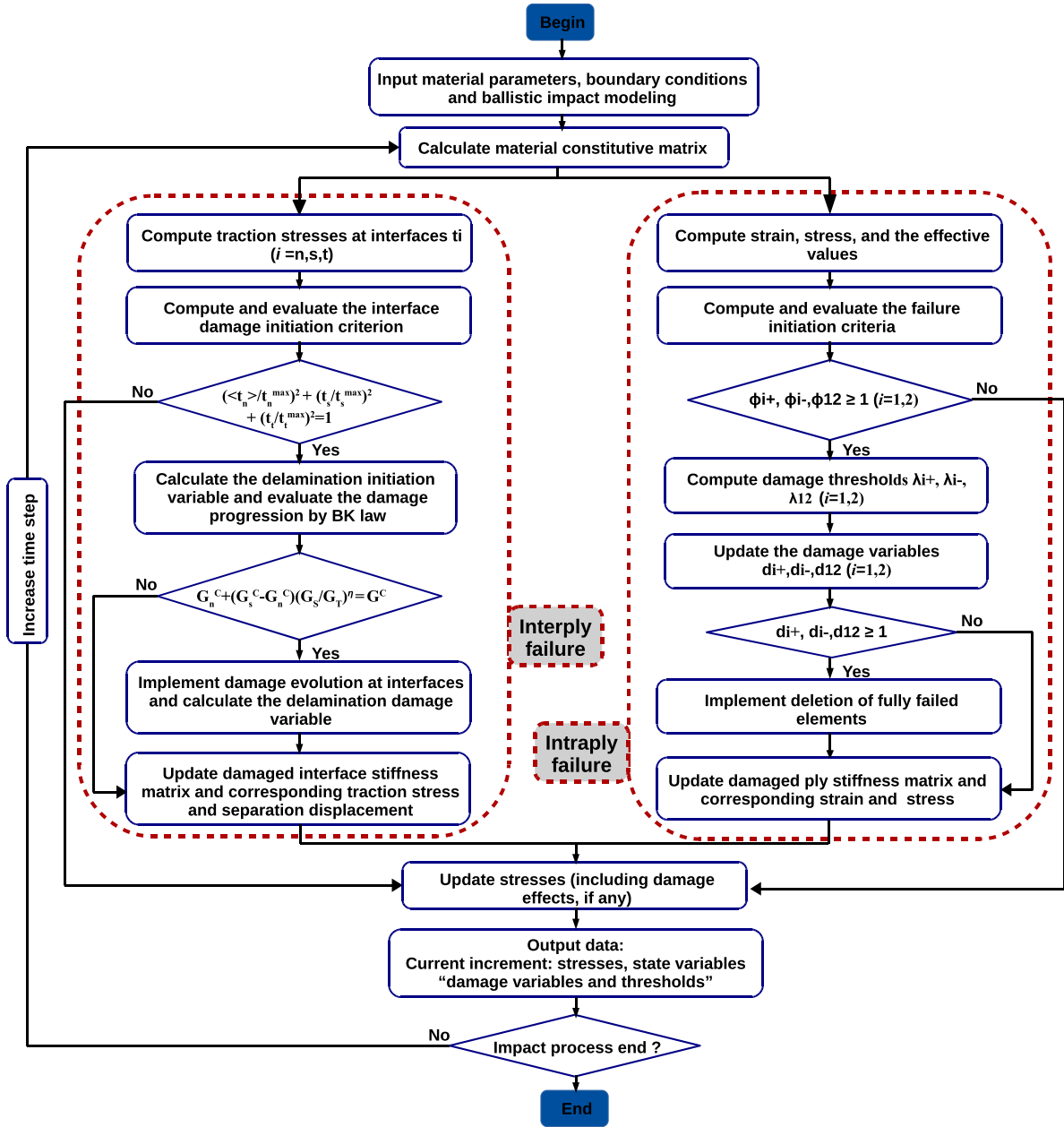
Begin

Input material parameters, boundary conditions and ballistic impact modeling

Calculate material constitutive matrix

Interply failure

Compute traction stresses at interfaces ti (*i* =n,s,t)

Compute and evaluate the interface damage initiation criterion

$(<t_n>/t_n^{max})^2 + (t_s/t_s^{max})^2 + (t_t/t_t^{max})^2 = 1$ — No / Yes

Calculate the delamination initiation variable and evaluate the damage progression by BK law

$G_n^C + (G_s^C - G_n^C)(G_S/G_T)^n = G^C$ — No / Yes

Implement damage evolution at interfaces and calculate the delamination damage variable

Update damaged interface stiffness matrix and corresponding traction stress and separation displacement

Intraply failure

Compute strain, stress, and the effective values

Compute and evaluate the failure initiation criteria

$\phi i+, \phi i-, \phi 12 \geq 1$ (*i*=1,2) — No / Yes

Compute damage thresholds λi+, λi-, λ12 (*i*=1,2)

Update the damage variables di+,di-,d12 (*i*=1,2)

di+, di-,d12 ≥ 1 — No / Yes

Implement deletion of fully failed elements

Update damaged ply stiffness matrix and corresponding strain and stress

Increase time step

Update stresses (including damage effects, if any)

Output data: Current increment: stresses, state variables "damage variables and thresholds"

Impact process end ? — No

End

Fig. 2. Flowchart of progressive failure analysis using the present ply-by-ply model for woven composite plies subjected to ballistic impact loading.

the energy used to suppress hourglass effects in bending dominated situations, should be minimal compared to the system internal energy (E_I), that is, less than 10%. In the case of large values of artificial strain energy, there will be a need to improve the mesh refinement or make other changes to the mesh.

Based on the initial velocity before impact (V_i) and exit or residual velocity (V_r) after perforation of the composite panels by the projectile of mass m_p, the following quantities can be calculated:

Amount of energy absorbed or dissipated by the composite panels at any given time t (E_{AB}) is expressed from (12) as $E_{AB}(t) = \frac{1}{2}m_p(V_i^2 - V_r^2(t))$

Velocity absorbed $(t) = V_i - V_r(t)$ (15)

%Energy dissipated

$= \left(\text{dissipated energy}(E_{AB})/\text{initial impact energy}\right) \times 100$ (16)

4. Validation of the present model

In the following, the developed ply-by-ply FE model is compared with data from other works to verify its reliability for different materials of the composite target. The experimental and analytical results reported in [49–51] are used to validate the FE model. In Ref. [49], experimental tests are carried out on E-glass/epoxy and carbon/epoxy composite targets. This set of experiments consist of four laminates, all with 8 plies. The first laminate is composed of 8 glass plies [G]₈, the second has 8 carbon plies [C]₈, the third is a symmetric hybrid laminate with exterior glass plies and interior carbon plies [G₂C₂]ₛ, and the last is a hybrid one with exterior carbon plies and interior glass plies [C₂G₂]ₛ. The dimensions of the tested laminates are 125 mm × 125 mm with a total thickness of 3 mm. The projectile has a cylindrical shape with a diameter of 6.36 mm, a length of 25.3 mm and a mass of 6.42 gr. The boundary conditions on the external edges of the laminate are constrained with an encastre constraint.

Table 1
Material properties adopted for modeling the damage and failure of the glass and carbon fabric reinforced epoxy plies.

Description	Glass/epoxy	Carbon/epoxy
Density (kg/m^3)	2100	1560
Elasticity constants		
Young's modulus 1-direction, E_1 (GPa)	24	56.813
Young's modulus 2-direction, E_2 (GPa)	24	56.813
Poisson's ratio, ν_{12}	0.108	0.047
Shear Modulus, G_{12} (GPa)	4.8	4.206
Damage initiation		
Tensile strength 1-direction, X_{1+} (MPa)	410	802.11
Compressive strength 1-direction, X_{1-} (MPa)	660	707.88
Tensile strength 2-direction, X_{2+} (MPa)	395	802.11
Compressive strength 2-direction, X_{2-} (MPa)	490	707.88
Shear strength S_{12} (MPa)	94	115.8
Damage evolution		
Tensile fracture energy 1-direction, G_f^{1+} (kJ/m^2)	65	44.9
Compressive fracture energy 1-direction, G_f^{1-} (kJ/m^2)	65	39.15
Tensile fracture energy 2-direction, G_f^{2+} (kJ/m^2)	65	44.9
Compressive fracture energy 2-direction, G_f^{2-} (kJ/m^2)	65	39.15
Maximum shear damage, d_{12}^{max}	1.0	1.0
Shear damage parameter, α_{12}	0.18634	0.18634
Shear plastic coefficients		
Initial effective shear yield stress, $\tilde{\sigma}_{y0}$ (MPa)	55	55
Hardening function coefficient, C	669.94	669.94
Hardening function exponent, γ	0.823	0.823

Table 2
Interply properties describing the initial stiffness of the interface, interply strength and fracture toughness.

	Mode I	Mode II	Mode III
Glass/epoxy			
Initial stiffness, K_i (N/mm^3)	10^6	10^6	10^6
Interply strength, t_i^{max} (MPa)	35.07	68	68
Interply fracture toughness, G_i^C (N/mm)	1.21	4.55	4.55
Carbon/epoxy			
Initial stiffness, K_i (N/mm^3)	10^6	10^6	10^6
Interply strength, t_i^{max} (MPa)	60	79.289	79.289
Interply fracture toughness, G_i^C (N/mm)	0.9	2.0	2.0

Table 3
Comparison between the numerical and experimental results for glass and carbon composite laminates.

Configuration	Ballistic limit velocity (m/s)		Variation (%)
	Experimental [49]	FE modeling (present)	
[G]$_8$	98	101.0	2.97
[C]$_8$	81	84.8	4.48
[G$_2$C$_2$]$_s$	87	89.6	2.91
[C$_2$G$_2$]$_s$	84	87.4	3.89

imental results reported in [49]. Table 3 illustrates the validation of the present FE model in terms of ballistic limit velocity with experimental results and good agreement has been observed with a percentage error of 2.91–4.48%.

To further validate the present numerical model, a new set of experimental and analytical results pertinent to kevlar reported in [50,51] are used. In Refs. [50,51], the residual velocities of a composite laminate target made of 12 plies of plain-woven fabric kevlar 29/epoxy are measured experimentally and calculated analytically. The dimensions of the target are 150 mm × 150 mm with a total thickness of 5 mm and the thickness of individual layer is 0.42 mm. The projectile is made of tungsten and has a cylindrical shape with a diameter of 10 mm, length of 20 mm and mass of 30.3 gr. The projectile is modeled as a rigid body considering the deformation of tungsten against composite negligible as indicated in [50]. The engineering constants and parameters of the failure criteria of the kevlar/epoxy lamina for the present validation are listed in Table 4. The elastic constants and strengths are taken from a corresponding material data in [50]. The intralaminar fracture energies per unit area under tensile and compressive loadings along the fiber directions of 44.9 kJ/m^2 and 39.15 kJ/m^2 respectively are chosen starting from the physical considerations concerning the values of other composite materials available in the literature [60]. The interface properties determining the delamination initiation between the surfaces are taken from [50] and listed in Table 4. The relevant critical energy release rates determining the failure response for interlaminar damage are obtained from [61]. The plastic behavior under in-plane shear is assumed based on the typical behavior of woven fabric reinforced epoxy laminates, the values are taken from [60].

Before the simulations are executed on the multilayer kevlar target, the mesh convergence is carried out to ensure the mesh independence of the results. The goal is to achieve the balance between the accuracy of the mesh and the computational time. The parameter considered for this assessment is the residual velocity of the projectile. The element size is varied from 0.5 mm to 2.5 mm with one element through the thickness for each ply. The results are compared when the laminate subjected to an impact velocity of 160 m/s. The residual velocity for each mesh size is obtained and the convergence is shown in Fig. 3. It can be seen that an element size of 1 mm is giving converged results of residual velocity. The further refinement does not lead to significant changes in the numerical results of the residual velocities. Therefore, a mesh size

The material properties that define the constitutive behaviors for modeling the damage and failure of both glass and carbon/epoxy plies are displayed in Table 1 [28,60]. The material parameters can be classified into four groups: elastic constants, damage initiation parameters, damage progression parameters, and shear plasticity coefficients. The elastic constants consist of the Young's moduli in the fiber directions 1 and 2, the Poisson's ratio, and the shear modulus (E_1, E_2, ν_{12}, G_{12}). The damage initiation parameters include the tensile and compressive strengths along fiber directions 1 and 2, and the shear strength at the onset of shear damage (X_{1+}, X_{1-}, X_{2+}, X_{2-}, S_{12}). The damage evolution parameters are evaluated from the fracture energies per unit area under tensile and compressive loadings along the fiber directions 1 and 2 (G_f^{1+}, G_f^{1-}, G_f^{2+}, G_f^{2-}) and by the parameters α_{12} and d_{12}^{max} introduced in eq. (6). Finally, the shear plasticity coefficients encompass the initial effective shear yield stress, $\tilde{\sigma}_{y0}$, and the hardening parameters C and γ in eq. (8).

On the other hand, to simulate the damage that may occur at the level of interfaces between composite plies, the material properties that define the constitutive behavior of these interfaces are considered. The interface properties of the simulated materials are obtained from [28,60] and given in Table 2. The interface initial stiffness (K_i) in Table 2 is chosen in such a way that ensures a quasi-rigid connection between the adjacent plies within the elastic regime. The critical energy release rates or fracture toughness values of interface bonds are essential for determining the damage propagation response for interply damage. It is generally assumed that the Mode III tearing fracture toughness (G_t^C) is equal to the Mode II interply shear fracture toughness (G_s^C), i.e., $G_s^C = G_t^C$.

The key indicator used here to evaluate the accuracy of the model, is the predicted ballistic limit velocity of the couple projectile-target, which is compared with the corresponding exper-

Table 4

Material properties of plain-woven kevlar/epoxy ply that are used for model validation [50].

Description	Kevlar/epoxy
Density (kg/m^3)	1440
Elasticity constants	
Young's modulus 1-direction, E_1 (GPa)	18.5
Young's modulus 2-direction, E_2 (GPa)	18.5
Poisson's ratio, ν_{12}	0.25
Shear modulus, G_{12} (GPa)	0.77
Damage initiation parameters	
Tensile strength 1-direction, X_{1+} (MPa)	1850
Compressive strength 1-direction 1, X_{1-} (MPa)	185
Tensile strength 2-direction, X_{2+} (MPa)	1850
Compressive strength 2-direction, X_{2-} (MPa)	185
Shear strength S_{12} (MPa)	77
Interply properties [50]	
Mode-I interlaminar normal strength, t_n^{max} (MPa)	34.5
Mode-II, III interlaminar shear strength, $t_{S,t}^{max}$ (MPa)	9
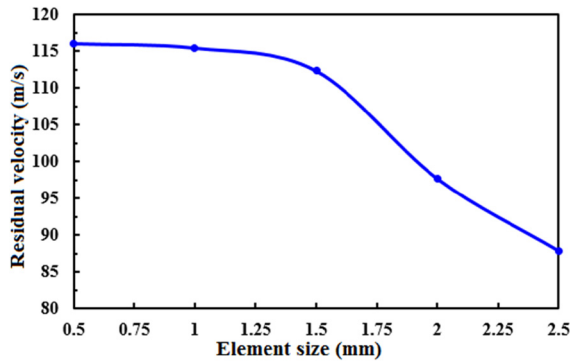
Fig. 3. Mesh convergence results.

of 1 mm is chosen for the current analysis and for further numerical modeling.

Fig. 4 shows a comparison of the predicted residual velocity at different strike velocities with the results obtained by experimental and analytical methods presented in [50,51]. The results show an overall good agreement between the predicted values from the developed FE model and those from other studies. Moreover, the ballistic limit predicted by the present model is 146 m/s, which is in close agreement with the experimental and analytical ballistic limit reported in [50] and [51] that are 143 m/s and 148 m/s, respectively. The ballistic limit is measured by determining the lowest impact velocity at which complete perforation occurs. The percentage discrepancy of the simulated ballistic limit velocity compared to the experimental and analytical ones does not exceed 2%. Furthermore, it is worth emphasizing that the experimental values are affected by an unexpected experimental variability, as depicted in Fig. 4. This is due to the effect of the non-zero impact yaw angle (the value in parentheses) that occurs during the ballistic tests (the impact is not perfectly perpendicular to impact surface). Knowing that in the FE simulation and analytical model, a perfect perpendicular impact condition is considered. It must also be taken into account that the present FE model is not able to reproduce the experimental results variability related to manufacturing issues of the composite fabrics. For example, as shown in Fig. 4, the experimental results close to the ballistic limit show a great variability in the residual velocity; although the K5#6 laminate is struck with a higher impact velocity than K5#5 laminate, but it is not perforated.

In order to further demonstrate the usefulness and accuracy of the present modeling approach, also the morphology of the damaged area around the impact point and the delamination among
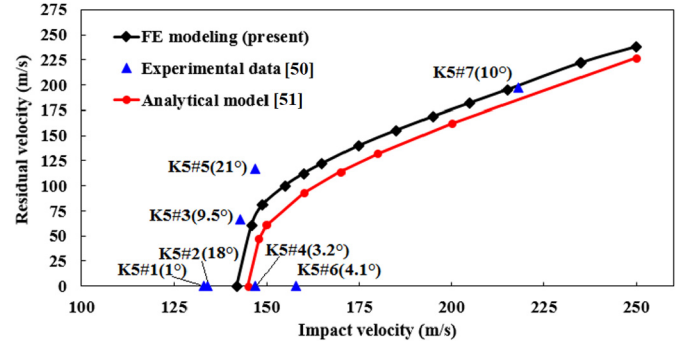
Fig. 4. Comparison between the residual velocities obtained from the present ply-by-ply FE model and other studies.

the layers are examined and compared to the experimental observations reported in [50]. In Figs. 5(a) and (b), experimental and FE results of the cases where the laminate underwent partial penetration (laminate K5#1) and full perforation (laminate K5#3) are compared. For both cases, the overall predicted failure patterns are in a good agreement with the experimental ones indicating an appropriate representation of intraply damage mechanisms within the model. Regarding the interply failure, the predictions are assessed by comparing the numerically predicted and experimentally observed interface damage. In case of full perforation, it can be seen that severe delamination occurs along all of the plies as shown in Fig. 5(b). Considering the partially penetrated state (Fig. 5(a)), it can be observed that the main delamination occurs in the plies that are perforated and the delamination degree in these plies is severe similar to that observed experimentally.

In general, the present modeling approach shows accurate results in predicting the ballistic impact of laminated composite panels, both for the quantitative, i.e. residual velocity and the qualitative analysis, i.e. delamination and damage morphology. Compared to the meso-heterogeneous approach employed in [50] which is considered impracticable due to the high computational effort required, the current approach involves much less computational cost. Besides, the present approach would provide a better understanding of the physical phenomena involved in the composite materials during impact loading, specifically of the damage features that can distinctively be characterized as tensile or compressive damage along fiber directions, matrix damage due to shear loading and interface damage or delamination. This subsequently gives rise to exploiting the developed FE model to study parameters not possible to detect by means of experimental tests as will be exemplified in the next section.

5. Results and discussion

In the present section, numerical simulations are conducted to comprehensively study the ballistic performance and damage behaviors of woven fabric laminate targets during ballistic impacts. The ballistic impacts are carried out at various impact energies and the impact responses are characterized based on the history curves of residual velocity and energy absorbed as well as damage progression and resultant damage shapes to evaluate the effect of impact energy on the damage behaviors. Initiation and propagation of interply debonding and the spatial distribution of damage at the impact location are the main features of the damage analysis performed in this study. Following that, parameters like stacking sequence, boundary conditions, interface properties including cohesive stiffness, interface strength and critical energy release rates on the ballistic performance of laminated composites are further investigated.
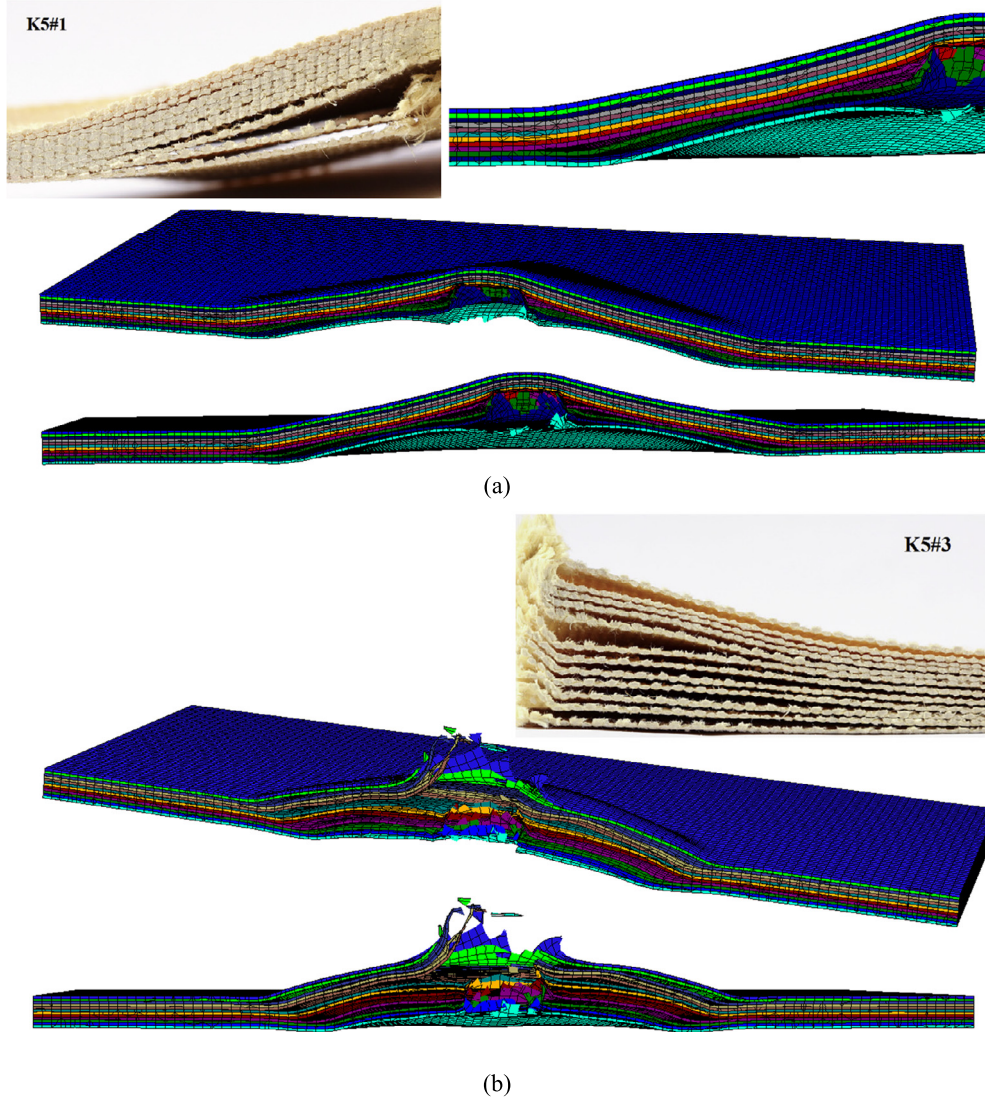
(a)

(b)

Fig. 5. Comparison of the numerically predicted failure patterns from the present model with experimental observations (a) partial penetration and (b) complete perforation.

For all cases in this section, we consider a 16-ply laminate target of size 150 mm × 100 mm with a total thickness of 4.8 mm. The plies are discretized with an element dimension of 1 mm × 1 mm × 0.3 mm. Moreover, the projectile is a flat-ended with a diameter of 16.5 mm, a length of 32 mm and a mass of 11 gr.

5.1. Ballistic performance and energy absorption mechanisms

In this subsection, the ballistic resistance of multilayered woven composite target with stacking sequence of $[+45/-45/0/90]_{2S}$ is investigated. Incident impact velocity of the projectile (V_i) is the primary stimulus that determines the nature of impact deformation and the level of damage on the target. Three incident impact velocities of 200 m/s, 300 m/s and 400 m/s are therefore assigned to the projectile to obtain the impact energies of 220 J, 495 J and 880 J, respectively. The variation of the projectile residual velocity versus time for the first impact scenario for the laminated target made of glass fabric plies is shown in Fig. 6. As depicted in Fig. 6(a), at incidence velocity of 200 m/s the target plate is not being perforated by the projectile. This means that the impact velocity is smaller than the ballistic limit state. In this case, the initial kinetic energy of the projectile is not adequate to perforate the target and the projectile rebounds back after it transforms all of its kinetic energy to the target. From

the velocity history, it can be seen that the projectile decelerates during impact until its velocity becomes zero (at 135 μs). At this time, the projectile retrieves kinetic energy through the elastic recover of the target and bounces back in the opposite direction and eventually accelerates to a constant negative value of −76.3 m/s. Moreover, after damage occurs in the target and when the projectile velocity passes through zero, the following states can be defined on the plot: Zone A corresponds to that the laminate moves forward faster and loses contact, Zone B represents that the laminate rebounds and catches projectile, contact is reestablished, Zone C corresponds to the projectile moving backward faster and losing contact again, Zone D indicates that the laminate bounces again and contacts the projectile, and Zone E represents the final bounce of the projectile from target where the contact is completely lost.

On the other hand, the history curves of projectile velocity during the ballistic impact of glass fabric laminate with incidence velocities of 300 m/s and 400 m/s are depicted in Fig. 6(b). The plots clearly show that the projectile decelerates during impact and then maintains a constant positive velocity after perforating the target. This indicates that the initial kinetic energy of projectile is more than the energy that the composite target can absorb. This, in turn, implies that for an impact velocity greater than the ballistic limit state, only a small amount of the projectile kinetic
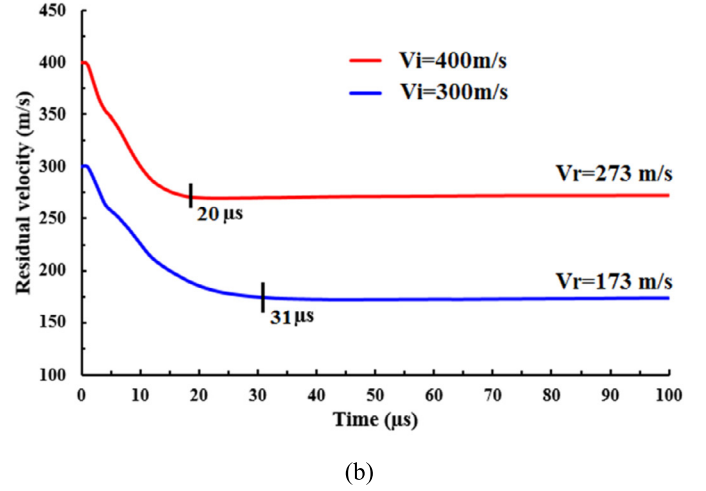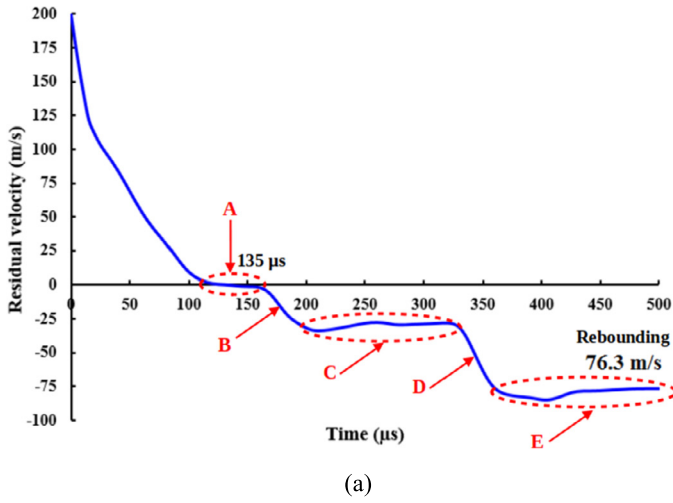
(a)

(b)

Fig. 6. Velocity history curve of the projectile during ballistic impact at incident velocities of (a) 200 m/s and (b) 300 m/s and 400 m/s for glass composite target.
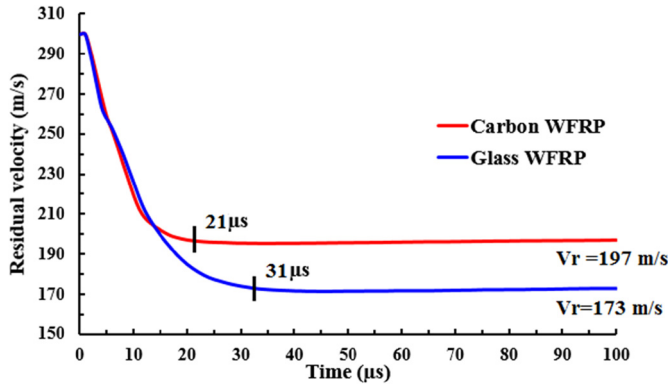

Fig. 7. Projectile velocity vs time for target of two different woven fabrics impacted at 300 m/s.

energy is sufficient to perforate the laminated target and projectile continues its moving across the laminate just like a rigid body at a constant residual velocity. At impact velocities of 300 m/s and 400 m/s, it can be seen that while perforating the target at about $t = 31$ μs and 20 μs, the projectile velocities become stable i.e., 173 m/s and 273 m/s, respectively.

It can be inferred from the above impact scenarios that the duration of contact increases with the increase in the initial impact velocity until ballistic limit at which the contact duration is maximum as the projectile travels a greater distance. A further increase of the velocity after ballistic limit gives rise to a reduction in contact duration because the projectile travels at a higher velocity and takes less time to pass through the thickness of the laminate. Among the three impact velocities, the perforation time for velocity of 400 m/s is the minimum.

Fig. 7 shows the variation of projectile residual velocity of two different woven fabric materials of laminated composite target to test which one has more resistance against perforation. Considering an impact velocity of 300 m/s, the residual velocity associated with carbon panels is almost 65.7% of the initial velocity, whereas the residual velocity for the projectile which impacts the glass panels is 57.6%. It is therefore easy to verify that the target made of glass fabric is the one which induces the highest reduction of the velocity of the projectile, because the residual velocity of the projectile is almost 12.2% lower in comparison with the value of carbon panels. The velocity absorbed by the carbon and glass composite panels are 103 m/s and 127 m/s, respectively.

In order to assess the resistance to impact loads and further explore the dynamic progressive failure behaviors, energy dissipation corresponding to different failure mechanisms of glass/epoxy target is investigated. Figs. 8(a)–(c) demonstrate the time histories of the total energy (E_T), internal energy (E_I), total kinetic energy ($E_{TK} = E_{RK} + E_{PK}$), and the energy due to viscous dissipation and friction at different impact energies of 220 J, 495 J and 880 J, respectively. At any time step during the analysis, it can be seen that the total energy of the system remains almost constant, as it should. This confirms the theory of energy conservation in the system and the appropriateness of the FE models developed to investigate the ballistic impact problem. As depicted in Fig. 8, at the beginning of the impact, the entire energy is in the form of kinetic energy of the projectile. Later, this energy is divided into energy absorbed by different damage modes and the kinetic energy of vibrated composite laminate and projectile. For the applied impact energy of 220 J, 495 J and 880 J, the ratios of the total dissipated energy to the initial kinetic energy of the projectile are about 100%, 66.7% and 53.4% (calculated by eq. (16)), respectively. As impact energy increases, more energy is dissipated, i.e., 220 J, 330.4 J and 470 J are the energies absorbed when the laminate is impacted by the latter three energies, respectively. These quantities are evaluated by eq. (12).

More generally, it is apparent from Fig. 8 that when the projectile begins to contact with the target, the total kinetic energy of the model starts to decrease which is due to that an amount of impact kinetic energy is absorbed by the laminate by different mechanisms resulting retardation of the projectile. Oppositely, the internal energy of the target rapidly increases as the impact progresses. The kinetic energy is transformed into the internal energy of laminate and dissipated energy due to vibration (E_{PK}), frictional (E_{FD}) and viscous (E_{VD}) effects. In Fig. 8(a) after time 190 μs there is an increase in the kinetic energy of the projectile because at this velocity the projectile did not perforate through the entire thickness and after the impact it bounces in the backward direction. As the incident impact velocity being very high, the projectile perforates the target at velocity greater than the ballistic limit and all dissipation terms become almost stable as can be seen in Fig. 8(c).

Fig. 9 shows the dissipation mechanism of kinetic energy of the glass/epoxy composite panels (E_{PK}) and the total internal energy (E_I) and its dissipation into E_{PD}, E_S, E_A and E_{DD}. For all impact scenarios, it appears that during the initial phase of contact, the internal energy (E_I) that develops in the panels due to impact overlaps with the recoverable strain energy (E_S). This reveals that in the initial stage, the developed internal energy is mostly
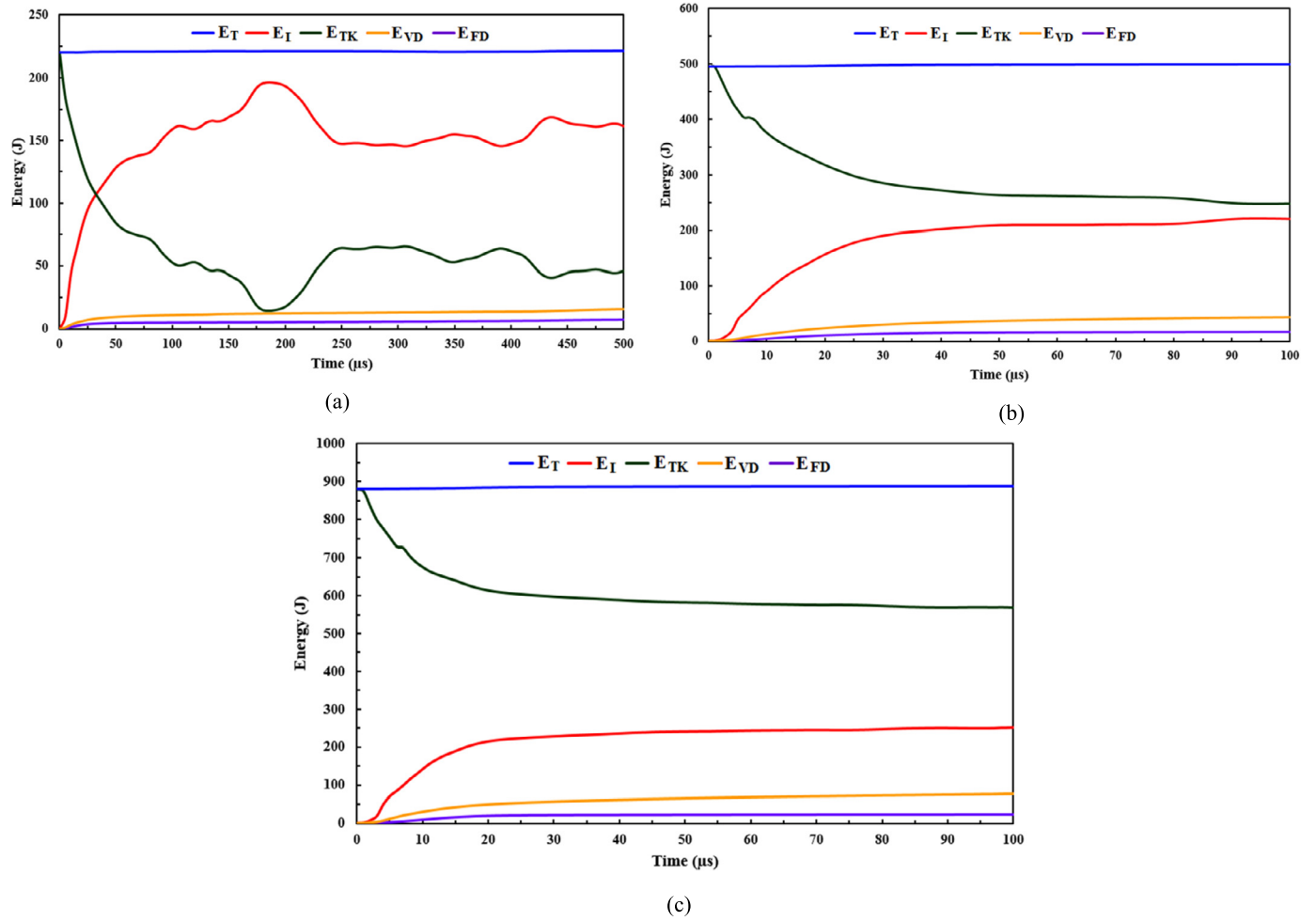
Fig. 8. Energy profile vs time at incident impact velocity of: (a) 200 m/s, (b) 300 m/s and (c) 400 m/s. (For interpretation of the colors in the figure(s), the reader is referred to the web version of this article.)

dissipated as recoverable elastic strain energy. Nevertheless, after development of other damage energy modes, i.e. E_{PD}, E_A and E_{DD}, the difference between the E_I and E_S becomes obvious. This result implies that some of the internal energy developed in the panels is dissipated as damage in the form of failure modes. Further, the artificial strain energy (E_A) is found to be less than 5% of the total energy for all modeling cases, indicating that the numerical models give stable solutions.

Of particular interest in the energetic analysis that plays an important role in the energy dissipation process, is the kinetic energy dissipation mechanism. By thoroughly examining the total kinetic energy of the entire model, it can be indicated that in addition to the projectile kinetic energy, there is another contribution provided by the vibration state of the composite target. As can be seen in Fig. 9, especially in high velocity impact situations, during the initial phase of contact, the gain in kinetic energy of the target laminate (E_{PK}) is more than the gain in internal energy. With the increase in the projectile velocity, the target deflection increases and as a result the target's kinetic energy increases and becomes a major energy absorption mechanism. It can also be seen that over time, the kinetic energy curves of the target decrease, due to the reduced vibration of the target panels as time progresses.

Moreover, it is of great importance to quantify the contribution of different energy absorbing mechanisms attributed to the glass/epoxy composite target. Fig. 10 illustrates the quantitative contribution of each individual energy absorbing mechanism mentioned before. It can be observed that overall, most of the energy due to impact is dissipated as inelastic deformation energy, kinetic energy of the target, elastic deformation energy and interlaminar delamination, with less energy being dissipated as frictional, viscous and artificial strain energy. More specifically, at low velocity of 200 m/s, 39.2% of the impact energy is absorbed as permanent inelastic deformation, 21.8% of the energy is dissipated as recoverable elastic energy, 8.5% by delamination damage, and 6.7% dissipates as kinetic energy of the target. On the other hand, at high velocity of 300 m/s, the contribution in energy absorption by inelastic deformation is 30%, by elastic strain energy is 25.5%, due to target kinetic energy is 25.5% and by delamination is 10.5%. On further increasing the velocity to 400 m/s, the majority part of energy absorption becomes in the form of kinetic energy of the target with 34% followed, successively, by the energy absorbed due to inelastic deformation, elastic strain energy and delamination by 26%, 14.8% and 9%.

5.2. Analysis of ballistic penetration process

Ballistic impact of the layered composite is a very complex phenomenon due to the complex nature of the ballistic penetration mechanism. It is considered as a transient dynamic process and its response is mainly governed by the local behavior of the material properties in the vicinity of the impact zone. In spite of the fact that the quantitative analysis previously performed in terms of residual velocity and energy dissipation indicates the ballistic performance of the target, the qualitative illustration of the fracture
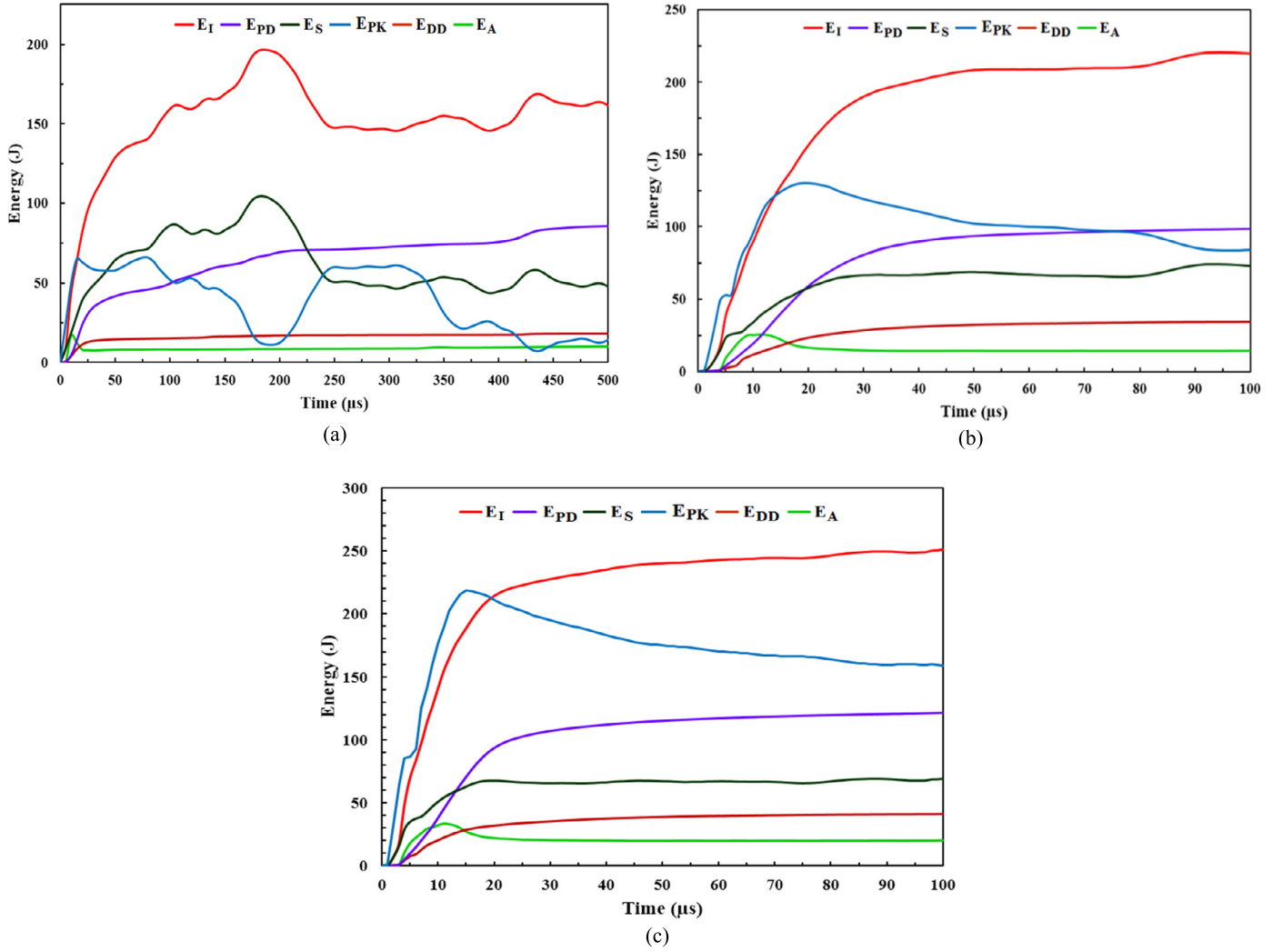
Fig. 9. Evolution of the target kinetic energy, internal energy and its dissipation modes at impact energies of (a) 220 J, (b) 495 J, (c) 880 J.

mechanism cannot be achieved by these quantitative values. By using the present ply-by-ply FE modeling approach, the deformation and damage propagation can be analyzed in detail throughout the ballistic penetration process. Fig. 11 illustrates the penetration process of glass/epoxy composite panels impacted by the previous three velocities (200 m/s, 300 m/s and 400 m/s). It is apparent that the impact damage and penetration mechanism below the ballistic limit velocity (Fig. 11(a)) is different from cases of higher velocity impact (Figs. 11(b) and (c)). As seen in Fig. 11(a), at impact velocity of 200 m/s, the target is not perforated and underwent partial penetration. In such a case, the projectile is intercepted and bounced back with negative velocity. This is in line with the discussion presented before where it was mentioned that at this velocity, the projectile is remained in the fragmented composite for long time causing an increase in deflection and subsequently the damaged material moves ahead of the projectile. The end of this impact event occurs after the projectile is stopped and reverted back from the target in the time range $t = 400$ μs to $t = 500$ μs.

Figs. 11(b) and (c) show the through-thickness damage development as a function of time for an impact of 300 m/s and 400 m/s. As depicted in these figures, the projectile penetrates the laminated target in a very short time. The impact contact lasts at time less than 100 μs, and different failure modes take place and couple with each other during the perforation process. Given the impact state in Fig. 11(b), the ballistic impact event can be divided into

different phases. During the initial phase ($t < 10$ μs), upon the impact-contact of the projectile with the laminated target, the material below the projectile undergoes compression, and as the projectile progresses, the material flows along the thickness direction. At time $t = 10$ μs, because of the further movement of the projectile due to the laminate compression, it results in bulging or cone formation on the back face. Between time $t = 10$ μs and $t = 20$ μs, the projectile continues penetrating the target with the growth of the bulge/cone and delamination. In the time range $t = 20$ μs to $t = 30$ μs, as the projectile moves further and under the lateral impact loading, a large bending deformation occurs and results in tensile failure of delaminated layers in the back of the laminate. When the fibers reach their tensile/compressive resistive tolerance, the fractures along the woven fabric directions take place. During time $t = 40$ μs to $t = 100$ μs, initiation of shear plug formation is observed and the continuous penetration leads to the complete plugging shear out of the laminate. During the last stage, the fragments are produced in the composite layers and splashed out into space.

5.3. Analysis of damage morphology and delamination

The attention here is focused on the qualitative aspects related to the morphology of the damaged area close to the impact zone and the delamination among the layers. In general, the damage and failure mechanisms in composite laminate are
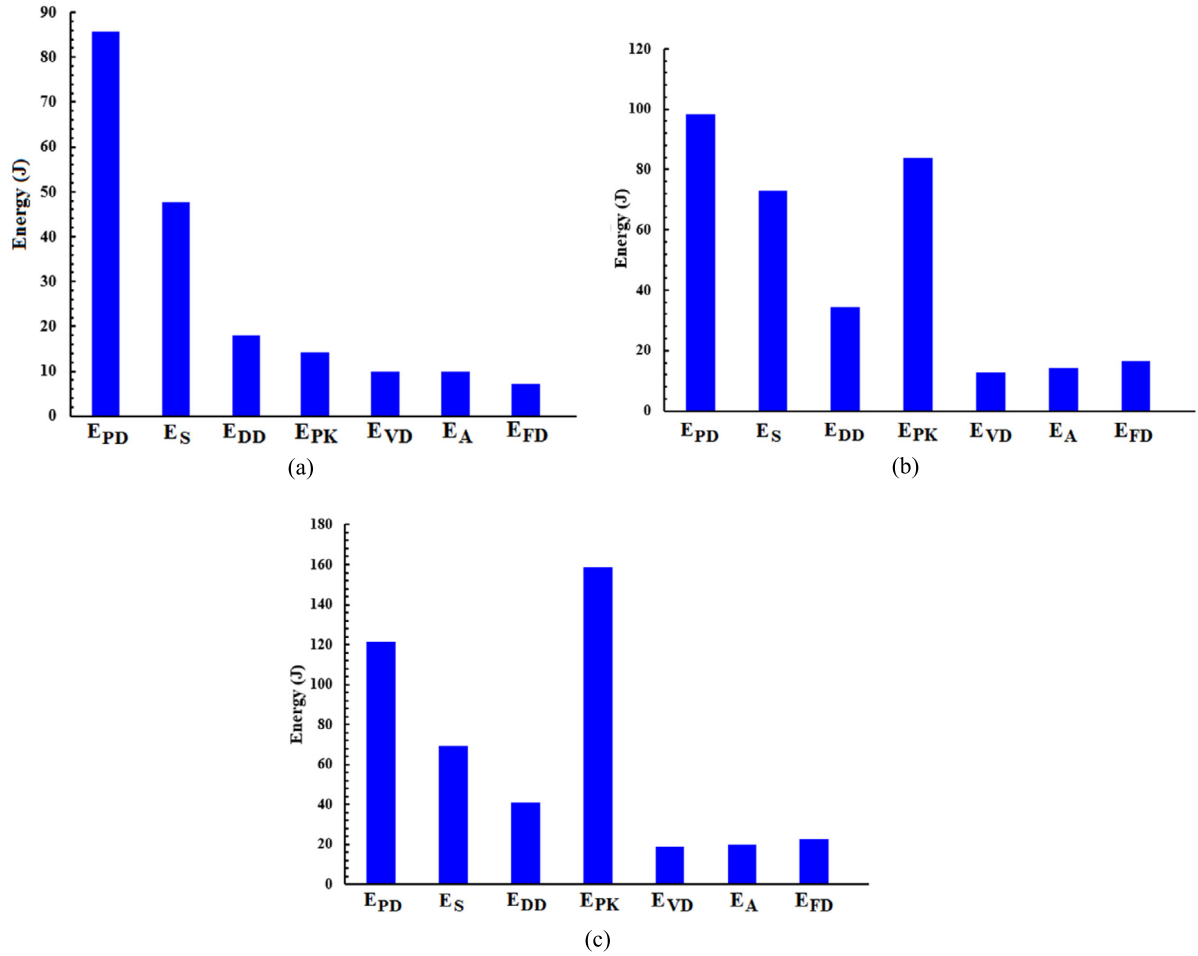
Fig. 10. Contribution of the different energy absorbing mechanisms at impact velocities of (a) 200 m/s, (b) 300 m/s and (c) 400 m/s.

more diverse, complicated, and characterized by different modes of failure, such as fiber breakage in tension and compression, matrix cracking, matrix plasticity and delamination of plies. It is more likely that all of these damage mechanisms contribute during the ballistic impact process. Therefore, it will be more convenient to identify the damage modes produced in the target during impact using the ply-by-ply FE model presented in Section 2.

Post-impact inspection of the laminated glass/epoxy target is carried out to identify the damage mechanisms arisen throughout the impact event at 300 m/s. Fig. 12 illustrates the damage evolution variables, including the tensile and compressive damage along the fiber directions ($d_{1\pm}$, $d_{2\pm}$), shear damage degree (d_{12}) and matrix plasticity due to shear in all the plies of the impacted target. The fully failed (damaged) materials are deleted from the model according to the element removal strategy and the red color in each ply indicates the higher damage level while blue color represents the intact material. It can be seen from Figs. 12(a)–(d) that the tensile/compressive damage in fiber directions 1 and 2 occurs severely in vicinity of the impact zone. With respect to the shear damage of the matrix, it is found that the damage variable d_{12} is comparatively insignificant, indicating that it has less effect on the failure of the composites under ballistic impact. More generally, it can be established from the contour plots that all damage mechanisms are most likely to occur, with fiber tensile damage is the predominant failure mechanism, followed by the mode of fiber damage due to compressive loading. Whereas the matrix shear failure mechanisms appear to be less important as depicted in Figs. 12(e) and (f).

Delamination damage is the most critical damage in the composite materials subjected to ballistic velocity impact. It can play a key role and dominant position in energy dissipation and damage of composite laminates under ballistic impact and can interact with matrix cracking. Fig. 13 shows the damage initiation and damage evolution for delamination mechanism through the thickness of the target laminate over a short time scale whereas its propagation in the in-plane direction as a function of time over a long time scale is depicted in Fig. 14. The initiation of the damage in the cohesive interaction is obtained by CSQUADSCRT variable (a value of 1 indicates initiation of delamination) while damage evolution can be tracked by CSDMG variable. The CSDMG parameter varies from 0 to 1 where 0 means no delamination and 1 implies complete delamination where the adjacent layers are no longer bonded by the matrix. For the short time scale, delamination initiates and grows though the thickness in the time range $3 < t < 10$ μs. At time $t = 3$ μs, the initiation of delamination predicted by eq. (10) occurs due to the transverse shear deformation around the projectile in the first few predefined interfaces. At time $t = 5$ μs, the projectile penetrates and initiation of delamination continues around the projectile until before the last two interfaces. At time $t = 8$ μs, delamination initiation at all interfaces is almost occurred and delamination evolution continues. Between $t = 8$ μs and $t = 10$ μs, as the projectile continues to penetrate into the target, the delamination continues to propagate in the in-plane direction.

For the longer time phase $15 < t < 80$ μs, the target undergoes large deformation and the extent of delamination in all plies is observed. The delamination reduces the bending stiffness of the tar-
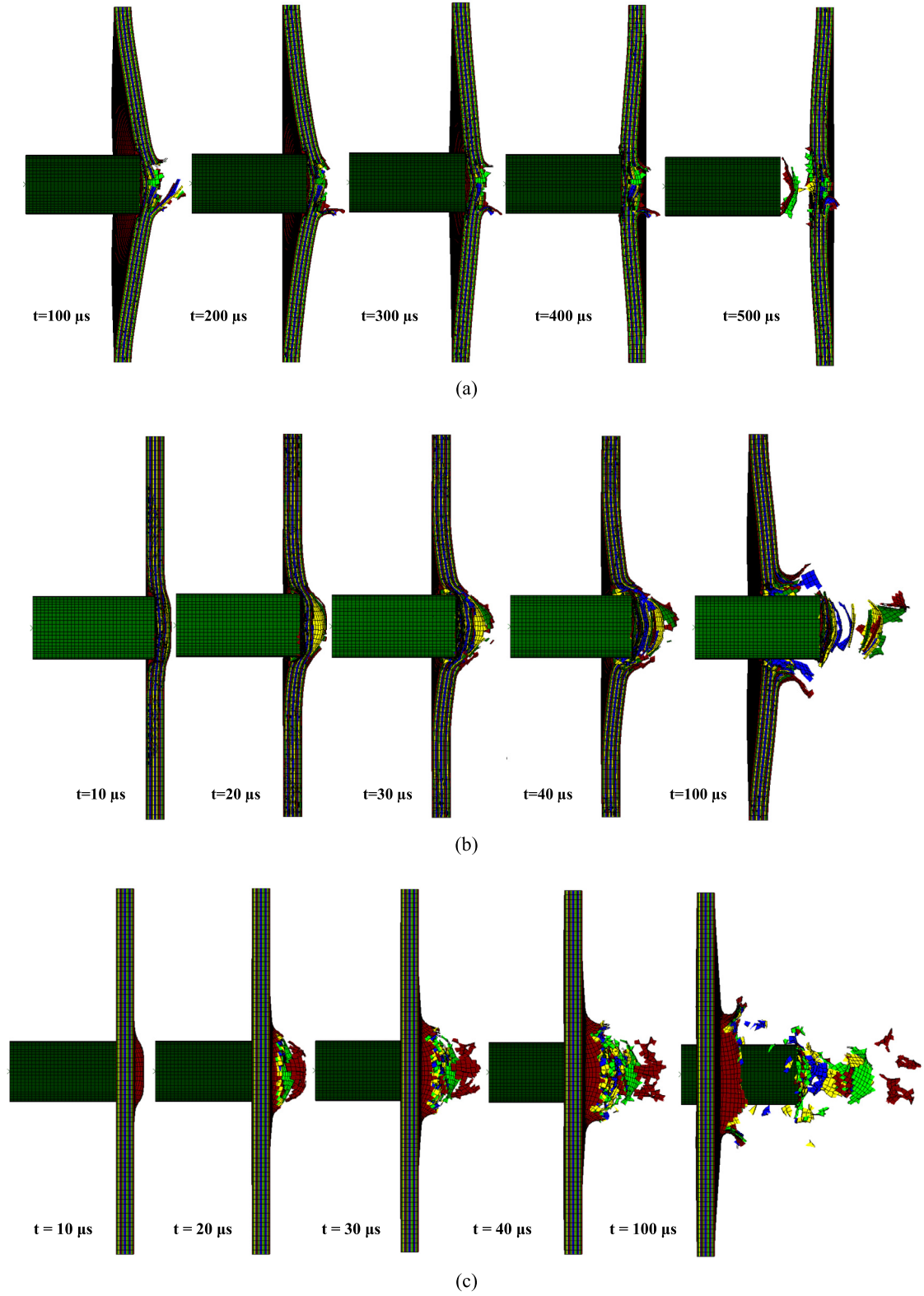
Fig. 11. Ballistic penetration process of glass/epoxy target at impact velocities of (a) 200 m/s, (b) 300 m/s and (c) 400 m/s.

get allowing local large deformation beneath the projectile, which reduces the target's penetration resistance. At time $t = 15$ μs, as the bulging of the back face grows, the delamination due to transverse shear deformation continues to grow. During time $t = 20$ to 80 μs, with large local tension-shear deformation due to the further projectile advancement, the growth of delamination is observed in addition to the tensile failure of the individual delaminated plies.

The above results demonstrate the potential of the present ply-by-ply model in providing the initiation and evolution of delamination in both the temporal and spatial domain, which otherwise cannot be acquired with any other experimental approaches.
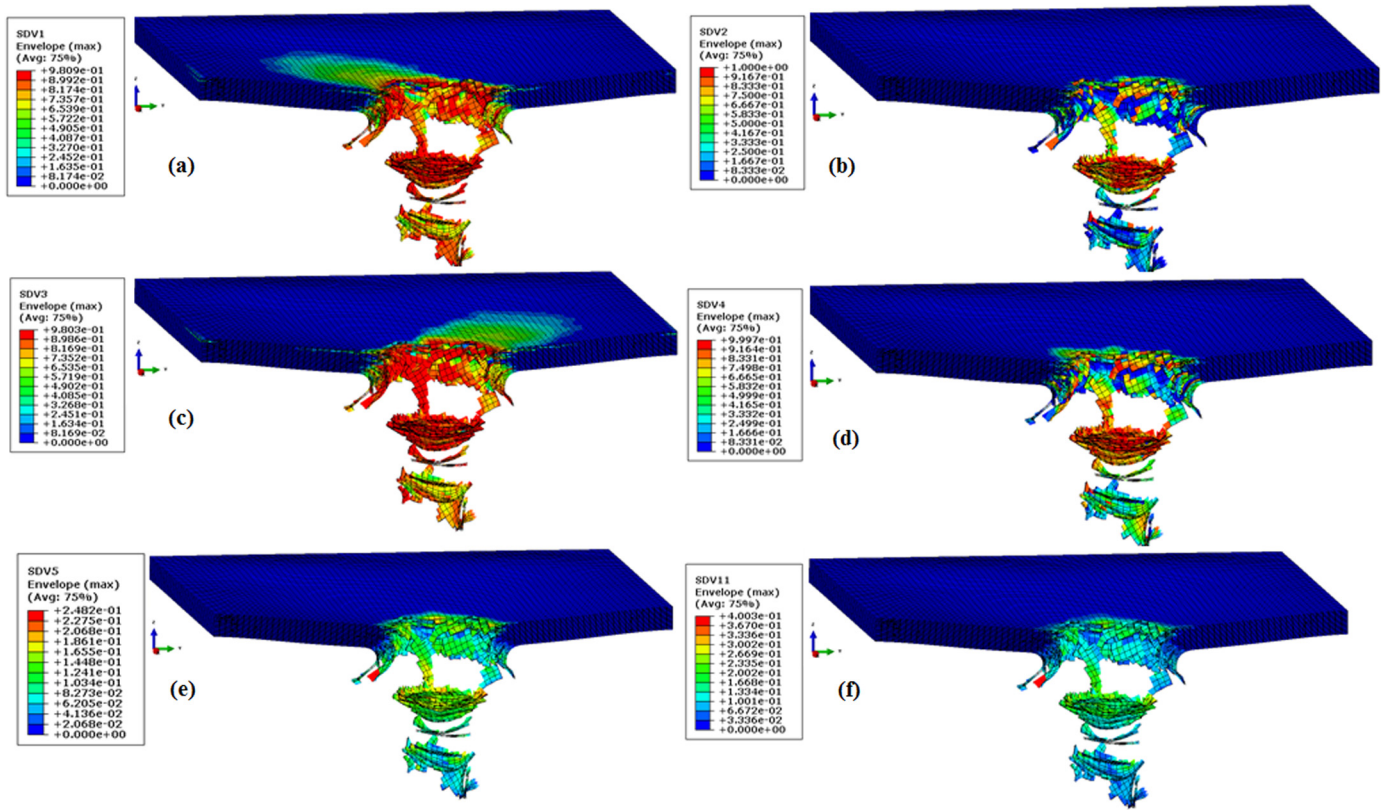
Fig. 12. Damage degree corresponding to (a) fiber tension along fiber direction-1, (b) fiber compression along fiber direction-1, (c) fiber tension along fiber direction-2, (d) fiber compression along fiber direction-2, (e) shear damage and (f) matrix plasticity under ballistic impact.
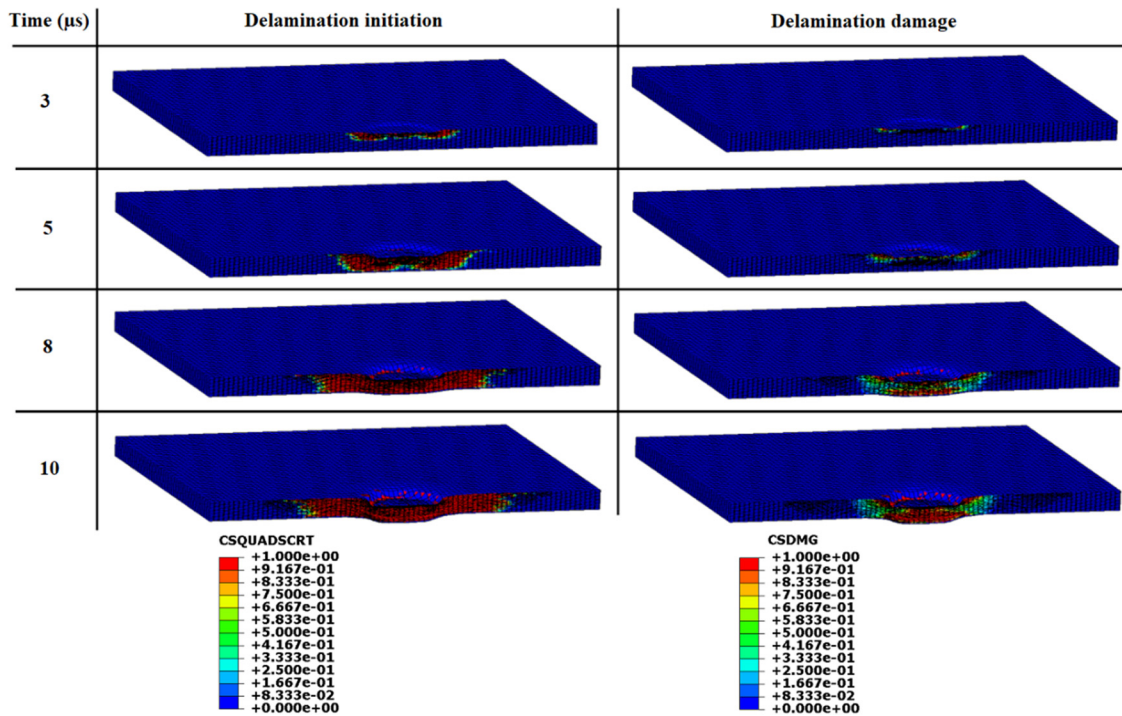

Fig. 13. Initiation and propagation of delamination over a short time scale at impact velocity 300 m/s. Blue color: intact material, green color: partial delamination, red color: initiation or full delamination.
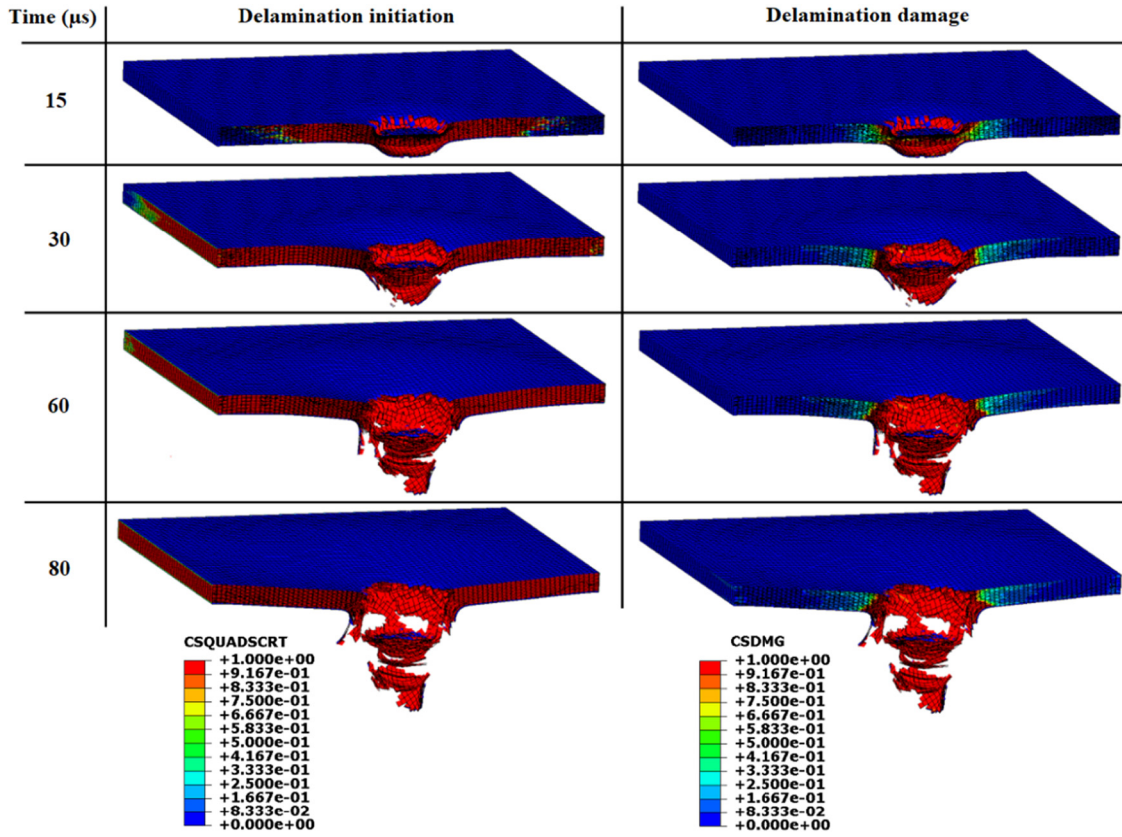
Fig. 14. Evolution of delamination as a function of time during long time phase at impact velocity 300 m/s. Blue color: intact material, green color: partial delamination, red color: initiation or full delamination.

5.4. Influence of ply-stacking sequence

In this subsection, a study of the influence of ply stacking sequence on the ballistic impact resistance of the laminated woven glass/epoxy target is performed. More specifically, we investigate the response of target configurations characterized by different stacking sequences subjected to a ballistic impact to estimate the influence on the velocity-time and energy-time histories. To do so, four different configurations are tested. The 1st configuration is the original one, used in previous analyses, configurations 2, 3 and 4 have the following lamination schemes $[45/-45]_{4s}$, $[0/90]_{4s}$, and $[0]_{16}$, respectively. For the four stacking sequences, Fig. 15 depicts the residual velocity of the projectile as well as the internal energy developed in the target during impact at incident velocity of 300 m/s. The residual velocity is a measure of ballistic penetration resistance of the composite laminates. As lower is the projectile residual velocity, more energy is lost and therefore more resistant is the composite target. This implies that the target absorbs more energy under various terms of energy absorption mechanisms as illustrated previously. Thereby the resistance to impact of the targets can also be assessed by the increase of internal energy, which is the more significant indicator compared to others. By inspection of Fig. 15, it is obvious that configuration $[0/90]_{4s}$ has the highest decrease in residual velocity compared to others and thus the higher increase in internal energy. Thereby this lamination scheme is the most impact resistant one. This can be explained by the fact that configuration with 0/90 oriented plies is more stiff in bending than other configurations making it more appropriate for lateral loads due to impact. Furthermore, comparing 1st configuration $[45/-45/0/90]_{2s}$ with the 2nd $[45/-45]_{4s}$, it is possible to conclude that there is no significant difference as is the case with the 3rd configuration $[0/90]_{4s}$.

The overlapped images of the intraply damage due to fiber tensile in directions 1 and 2 (the predominant failure mechanism) throughout the whole lay-up, for the considered stacking sequences, are reported in Fig. 16 from its impact sides. Through these observations, there is a clear effect of stacking sequence for composite laminates in terms of impact induced damage pattern. From Fig. 16, it is evident that the tensile damage is developed mainly along the fiber directions and the damage shape is affected by the fiber orientation of the laminates. Also, it should be noted that the damage pattern of the laminates ($[45/-45/0/90]_{2s}$ and $[45/-45]_{4s}$) is different from those of other laminates ($[0/90]_{4s}$ and $[0]_{16}$ and this is mainly due to the fact that the tensile damage is apparently higher along the corresponding fiber directions, which tends to result in the tensile failure. The damage distribution directions are aligned to the fiber orientations.

5.5. Analysis of the target boundary conditions

The studies regarding the influence of target boundary conditions on ballistic resistance are very limited and needs further investigation. Numerical results are presented and discussed to describe the influence of target boundary conditions on the ballistic resistance by impacting the projectile on the glass/epoxy laminate with all the four edges clamped (C-C), two opposite edges clamped and two free (C-F) and the four edges simply supported (S-S). Fig. 17 describes the effect of different support conditions on the ballistic resistance in terms of projectile residual velocity at incidence velocity of 300 m/s. As can be seen, the influence of boundary conditions on the energy absorbing capacity of the target is minimal. The differences in the residual velocity, due to the change in boundary condition from C-C to C-F and C-C to S-S, decreased by 1 m/s and 0.8 m/s, respectively. This implies that the
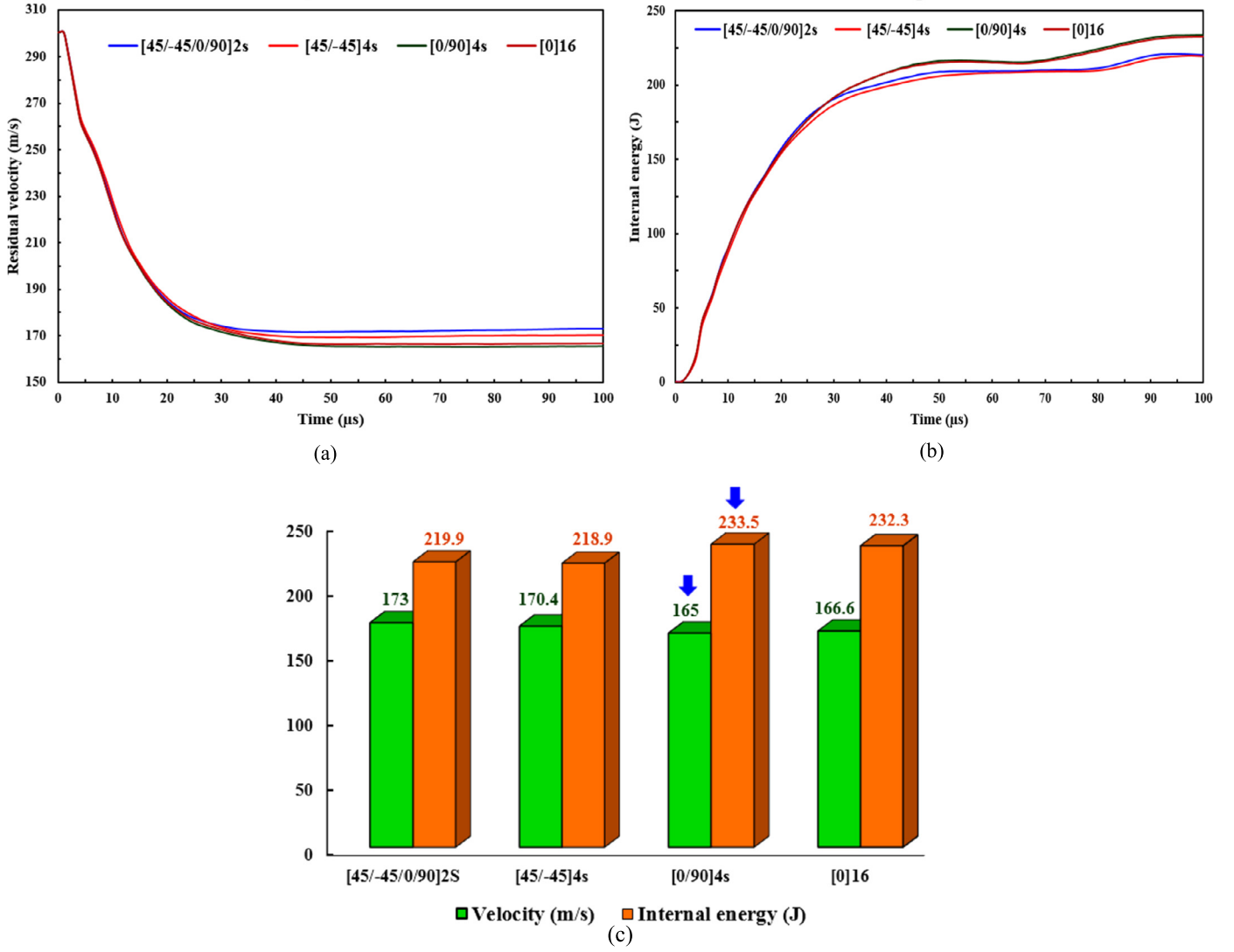
Fig. 15. Time histories at 300 m/s of (a) residual velocity and (b) internal energy for different stack-up sequences. (c) An illustration of both residual velocity and internal energy at the end of the impact event.

ballistic resistance offered by the target is slightly higher corresponding to clamped free and simply supported boundary condition than the fully clamped boundary condition. As shown in Fig. 17, for the C-F boundary condition, due to the lower stiffness at the boundary, there is more deflection in the target and the target experiences more vibration due to elastic wave propagation that causes more ballistic resistance because of the absorbed energy by kinetic energy corresponds to the vibration of the panels.

From the above results, it can be revealed that the ballistic performance of the laminated target is slightly influenced by imposed boundary conditions. This may be due to the relatively small contact duration between the target and the projectile. As considering the boundary condition, in general, the ballistic resistance of the target in terms of the projectile residual velocity increased little bit with imposed boundary condition changes from C-C to C-F, followed by S-S.

5.6. Analysis of interface properties

5.6.1. Effect of interface stiffness K_i

We aim here to study the influence of adhesive interface parameters on the overall composite target behavior and then on the

amount of dissipated energy due to interply delamination damage. First, the interface property that determines the initial stiffness of the interface K_i is examined. This parameter is obtained under the assumption that the interface is a quasi-rigid connection within the elastic regime with high initial penalty of $K_i = 10^6$ MPa/mm for fracture mode I, II, III. The effect of decreasing this parameter on the overall target response of the glass/epoxy in terms of residual velocity and energy dissipated by delamination is displayed versus time in Fig. 18 at a strike velocity of 300 m/s. As shown in Fig. 18, a decrease in the cohesive stiffness from $K_i = 10^6$ MPa/mm to $K_i = 10^2$ MPa/mm results in an increase in the residual velocity of the projectile by about 18.5% and a decrease in energy dissipated by the delamination mechanism by about 85%. From this result, we can infer that the enhancement of the interface penalty stiffness within certain limits could improve the resistance to penetration, and thus lead to lower residual velocities. Such improvement can be attributed to the delay in the initiation of damage (delamination) and thus retarding the degradation of cohesive stiffness due to the increased interface stiffness. Since the onset of delamination growth is correlated to interface stiffness as explained in Section 2, before the damage initiates, the interface is intact and when has a large initial penalty stiffness, the delamina-
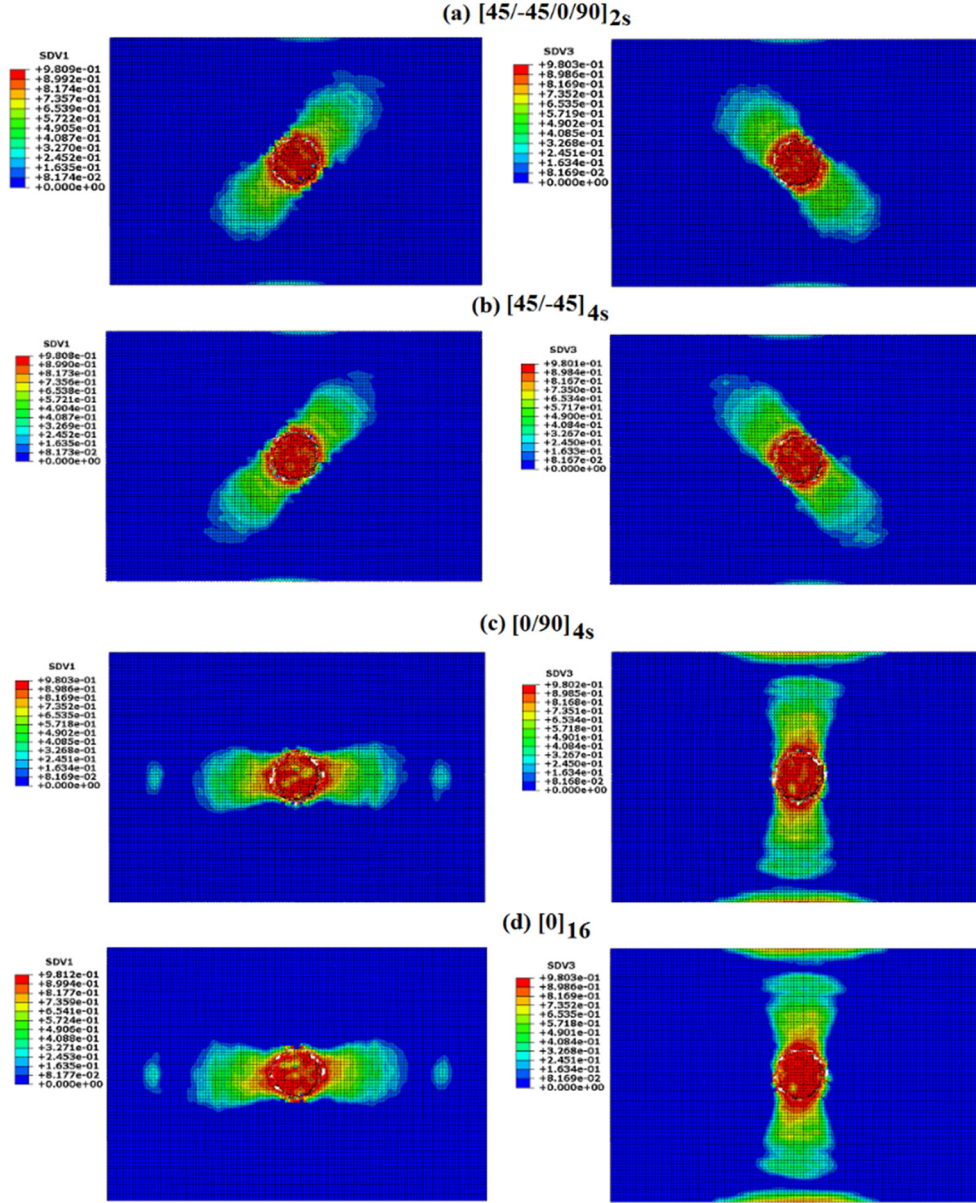
Tensile damage along fiber directions 1 & 2

(a) [45/-45/0/90]$_{2s}$

(b) [45/-45]$_{4s}$

(c) [0/90]$_{4s}$

(d) [0]$_{16}$

Fig. 16. Influence of stacking sequence on the intraply damage patterns at impact velocity of 300 m/s.
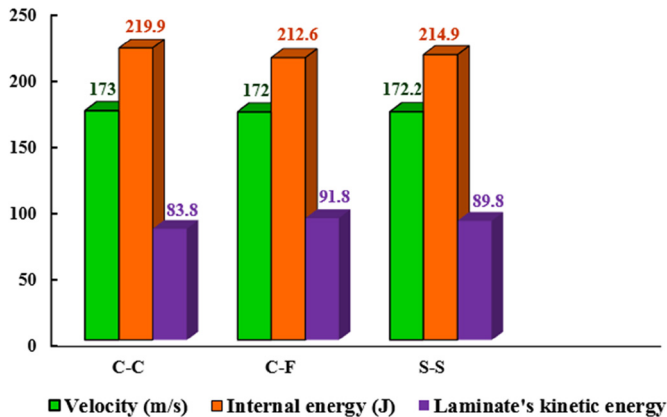

Fig. 17. Influence of boundary conditions on the ballistic resistance.

tion initiation is delayed and ultimately leads to more dissipated energy.

5.6.2. Effect of interply strength (t_i^{max}) and fracture toughness (G_i^C)

Second, the cohesive interface properties t_i^{max} (interlaminar strength) and G_i^C (critical fracture toughness) of fracture mode I, II, III are then investigated and the results are shown in Fig. 19. Simulation result with the interface properties of glass/epoxy laminate in Table 2 is used as the baseline (case 1 in the figure). The values of t_i^{max} and G_i^C in cases 2 and 3 are both increased by 50% and 100%, respectively. In case 4, the values of t_i^{max} and G_i^C are reduced by 50%. From the history curve of residual velocity of the projectile shown in Fig. 19(a), it can be seen that the residual velocity is strongly correlated to both the interface strength and fracture toughness properties. The residual velocity is decreased by about 6.6% and 11.5% when the interface properties are increased by 50% and 100%, respectively. Conversely, when the interface parameters are decreased by 50%, the residual velocity is increased by about
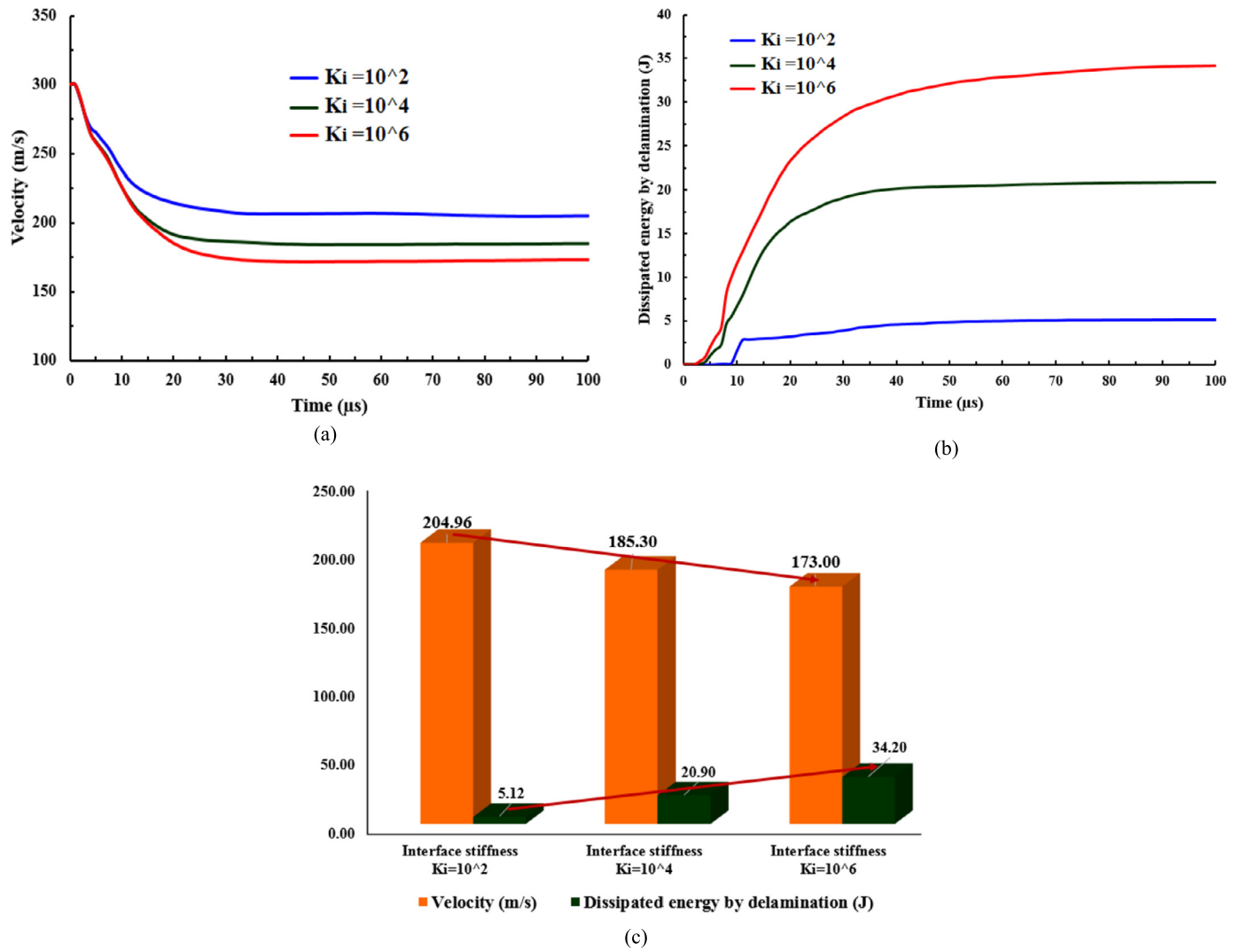
(a)

(b)

(c)

Fig. 18. Effect of interface stiffness K_i on the residual velocity and energy absorbed by delamination of plies at an incident velocity of 300 m/s.

3.8%. Similarly, it is possible to obtain a quantitative perspective of the amount of energy absorbed by delamination. As illustrated in Fig. 19(b), the energy absorbed by delamination damage is sensitive to the interface properties. When the interface parameters are increased by 50% and 100%, the amount of energy absorbed by delamination is increased by about 19.7% and 31.5%, respectively, while reducing the interface properties by 50% results in a decrease in the delamination absorption capacity by about 22%. In the meantime, it is worth noting that the dissipation energy due to damage caused by interply delamination is extremely important, and remains still comparable with other energy dissipation modes.

Considering the damage morphology associated with the interface parameters used in cases 1, 2 and 4, the projected areas of interply delamination damage are plotted for the interfaces 5, 7, 11, 13 and 16 in Fig. 20. From these patterns, it can be seen that the predicted damage evolution parameter is positively correlated to the delamination interface properties. At low values of t_i^{max} and G_i^C (−50%, left), the largest delamination damaged areas are pronounced. Comparatively, at high values of interface parameters (+50%, right), delamination areas are confined to a small zone localized around the perforated hole border. The difference in the delamination damage spread is certainly attributed to the resistance offered by laminate due to the increase in interlaminar interface strength and its critical fracture toughness properties.

5.6.3. Interface parameters in shear (Mode II, III) versus tensile (Mode I)

To get information about the sensitivity of ballistic performance in relation to the interface parameters used for normal and shear failure modes, further simulations are required. In order to distinguish between the influence of normal failure parameters (fracture Mode I) and shear failure parameters (Mode II, III) on target ballistic resistance in terms of residual velocity and energy dissipated due to delamination of plies, three different combinations of t_n^{max}, G_n^C and $t_{s,t}^{max}$, $G_{s,t}^C$ are studied. The first set with ($t_n^{max} = 35.07$, $G_n^C = 1.21$) and ($t_{s,t}^{max} = 68$, $G_{s,t}^C = 4.55$) is used as the baseline. In the second case, the values of ($t_{s,t}^{max}$, $G_{s,t}^C$) are increased by 100% while t_n^{max}, G_n^C remain as in the first group. In the third case, the values of t_n^{max}, G_n^C are increased by 100% while $t_{s,t}^{max}$, $G_{s,t}^C$ remain unchanged. Fig. 21 shows the dependence of the residual velocity as well as the dissipation energy by delamination on the interface strength and critical fracture toughness parameters. The trend is more sensitive to interface parameters in shear fracture (Mode II, III). The results show that when values of the shear adhesive $t_{s,t}^{max}$, $G_{s,t}^C$ are increased by 100%, the residual velocity is decreased by about 5.7% as the amount energy dissipated by the delamination increases by about 22.9%. On the contrary, the ballistic performance is insensitive to increas-
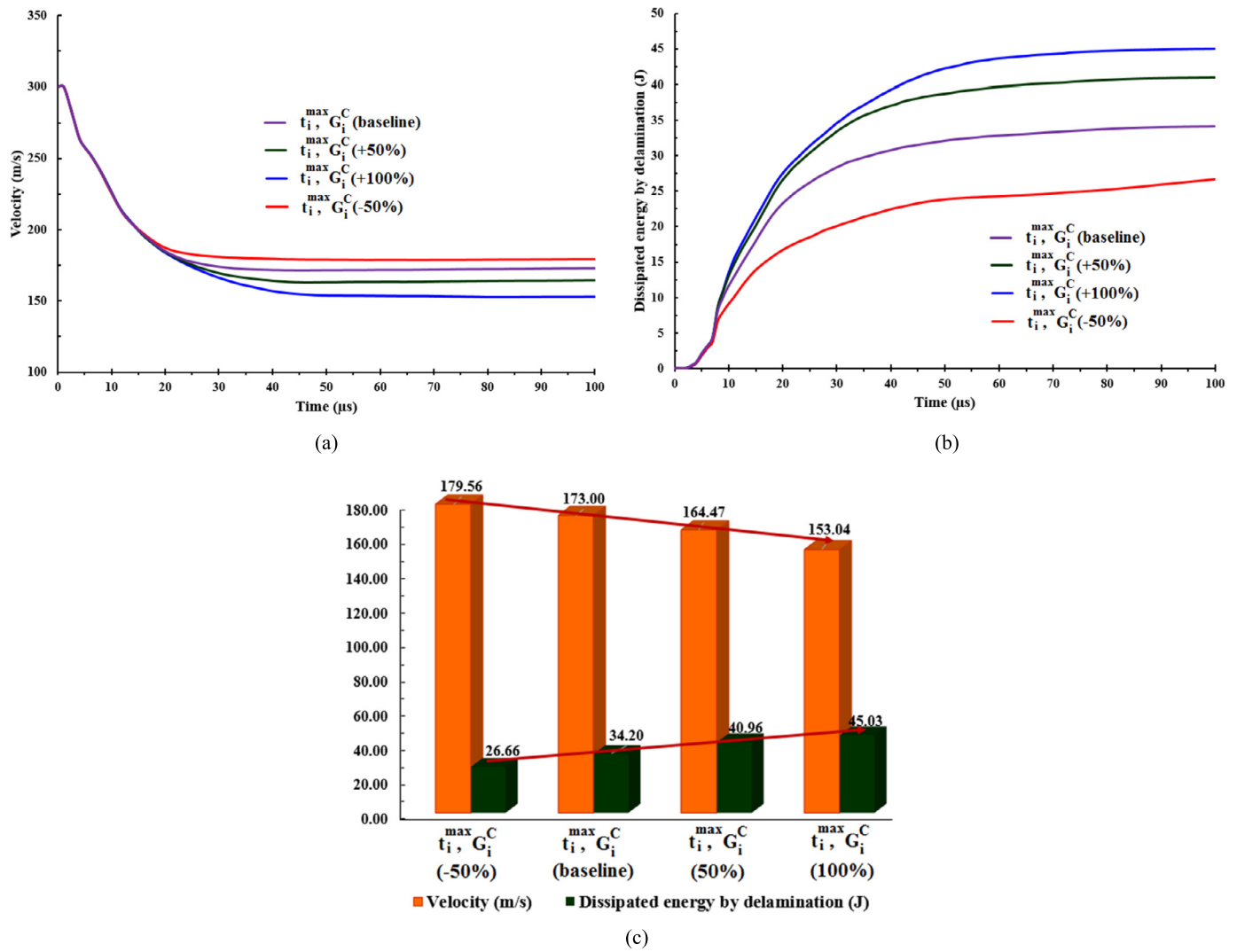
(a)

(b)

(c)

Fig. 19. Effect of interply strength and fracture toughness parameters on residual velocity and energy dissipation due to delamination.

ing interface strength and fracture toughness in normal failure mode.

From the above, we can infer that the present sensitivity analysis has found the global internal energy trend to be sensible to the adhesive parameters since the contribution of these parameters does affect the global energy balance and projectile residual velocity trends.

Considering the delamination pattern associated with the interface parameters in the shear (Mode II, III) and tensile (Mode I) used above, the projected areas of interlaminar delamination damage are depicted for the interfaces 5, 7, 11, 13 and 16 in Fig. 22. From these morphologies, it can be noticed that the predicted damage evolution parameter (CSDMG) is more sensitive to interface parameters in shear fracture (Mode II, III) than in tensile (Mode I). When the values of shear adhesive $t_{s,t}^{max}$, $G_{s,t}^C$ increase by 100%, the smallest delamination damaged areas can be observed. On the other hand, at higher values of interface normal failure t_n^{max}, G_n^C (100%), the degree of delamination growth is less influenced as little change in delamination damage spread is observed.

Thus far, the adoption of such numerical modeling approaches has permitted to derive and understand the constitute relationship, interpret of the effect of each considered parameter and simulate the overall ballistic materials behavior in response to ballistic impact. This ultimately gives rise to an effective design for an enhanced ballistic resistant composite target. Besides, given

the heterogeneous nature of the laminated composite with its various material characteristics, the nature of stress and strain, and interaction between intraply and interply failure, it was absolutely necessary to have a thorough understanding of the various parameters influencing the ballistic impact response of the composites in order to develop the most optimized configuration. To that context, the parameters studied were material-based and include the type of fiber materials and interface systems, and geometry-based such as stacking sequence and boundary conditions.

6. Conclusion and final remarks

The scope of this work was to propose a computational framework for modeling the ballistic impact of woven laminated composite materials. This framework has addressed the failure modes and predicted the damage response in laminated composites under ballistic perforation impact. The material responses with large nonlinear behavior due to fiber rupture, matrix cracking, and plasticity effects due to micro-matrix cracking under shear loading were accounted for. The intraply damage model was implemented using ABAQUS/Explicit user defined material subroutine VUMAT and the interply delamination was simulated by a damage surface-based cohesive contact model. In order to verify the validity and accuracy of the developed FE model, an initial numerical study
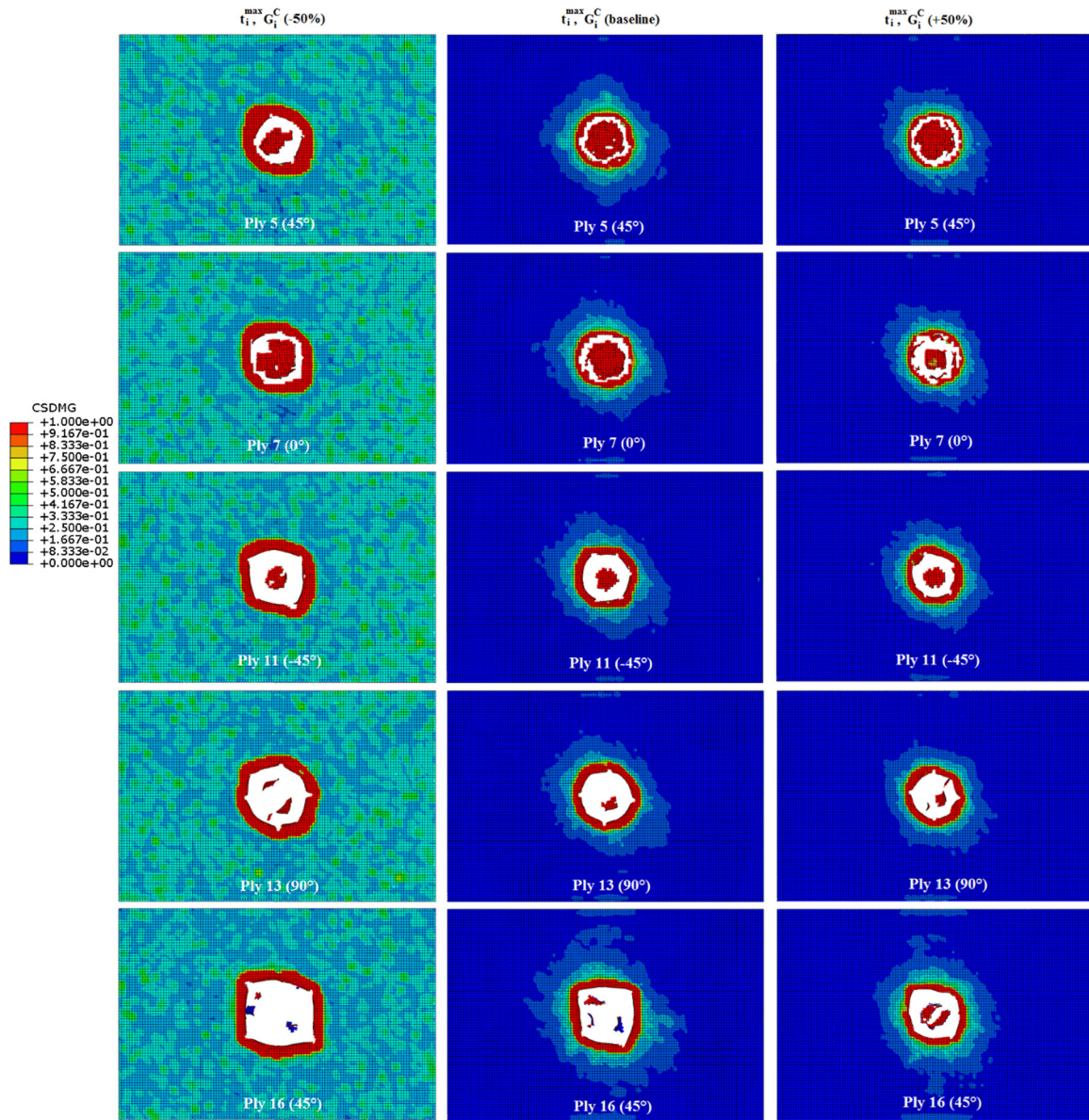
Fig. 20. Degree of delamination growth influenced by delamination interface properties (t_i^{max} and G_i^C). Red areas indicate complete interply delamination, blue refers to no delamination and green indicates partial delamination.

was conducted on the response of composite laminate targets under high velocity perforation. Overall, it was transpired that the present model predicts well the experiments in terms of damage morphology, delamination pattern and residual velocity for high velocity impact. Further, the results presented in the current study gave an insight into the influences of the considered parameters on the ballistic performance in terms of residual velocity and energy absorbing mechanisms. Based on the constitutive material models development procedure used and the results of the subsequent computational analyses, the following main conclusions can be drawn:

1. The study shows that the modeling strategy based on the continuum shell elements of the individual plies in conjunction with the surface-based cohesive zone model of the interlayer allows the computational effort to be kept within reasonable bounds.

2. The present model predicts well the experiments not only in terms of residual velocity but also in terms of damage patterns and delamination in the case of partial penetration and full perforation. This makes the model suitable for use with confidence to simulate numerically projectile impact on woven laminates in a wider range of velocities. In terms of ballistic limit velocity, validation of FE models against experimental results showed good agreement with a percentage error of 2–4.48%.

3. The duration of contact plays an important role in ballistic impact; it increases as the initial impact velocity increases up to the ballistic limit velocity and decreases thereafter. As a result, the damage mechanisms were found in the glass/epoxy target varying before and after the ballistic limit velocity. At high impact velocities of 300 m/s and 400 m/s, it was found that while perforating the target at short times of about $t = 31$ μs and 20 μs, the projectile velocities become stable i.e., 173 m/s and 273 m/s, respectively.

4. At a velocity lower than the ballistic limit (200 m/s), most of the energy was absorbed in the form of inelastic deformation (39.2%), followed successively by the elastic strain energy stored within the target (21.8%), interlaminar delamination (8.5%), and kinetic energy due to panels' vibration (6.7%).
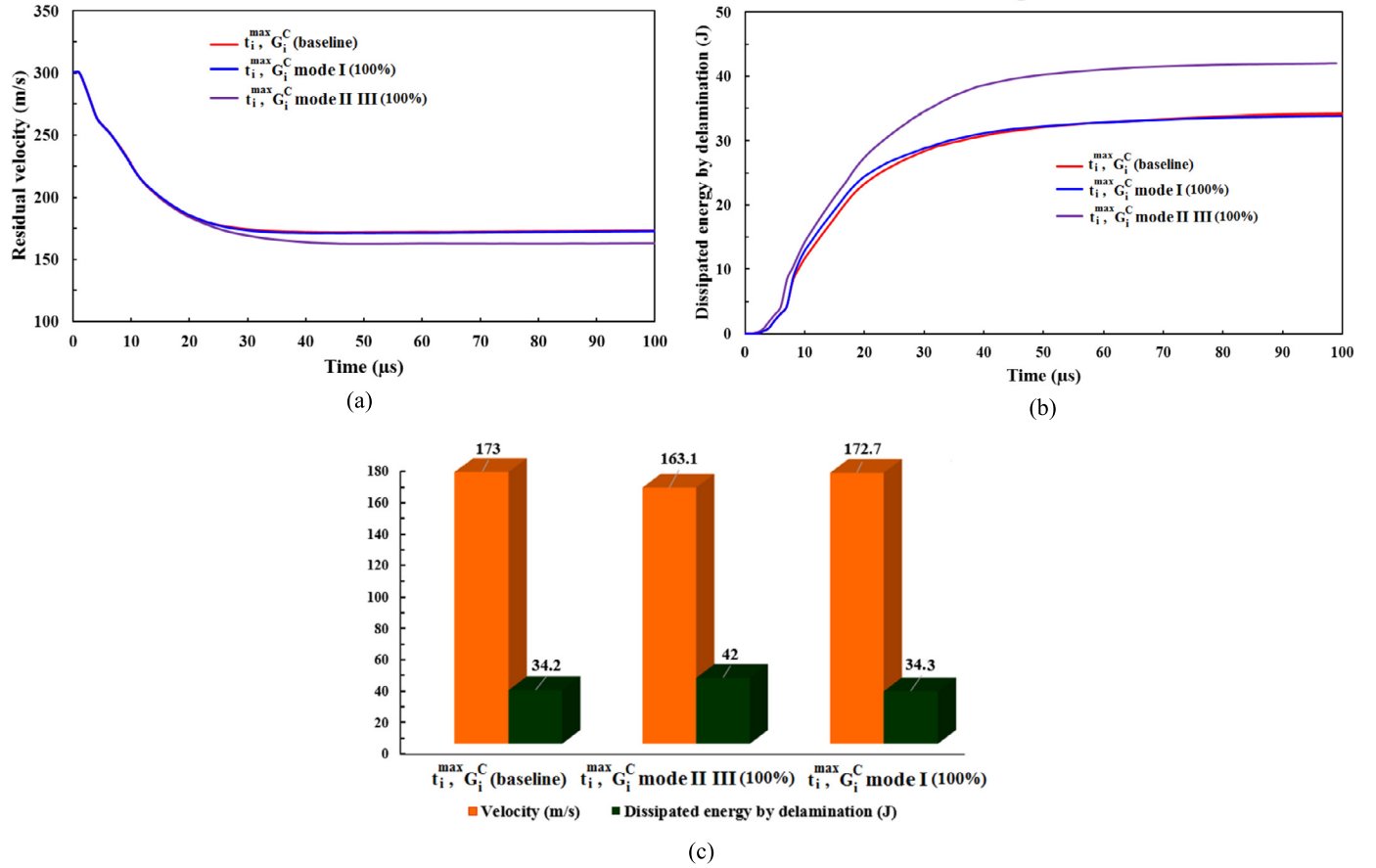
Fig. 21. Influence of delamination strength and fracture toughness parameters of Mode I, II, III on (a) residual velocity and (b) energy dissipation due to delamination at impact velocity of 300 m/s. (c) An illustration of both residual velocity and dissipated energy by delamination at the end of impact process.

On the other hand, at a high perforation velocity of 400 m/s, the majority part of energy absorption became in the form of the target's kinetic energy (34%) followed, respectively, by the energy absorbed due to inelastic deformation (26%), recoverable elastic strain energy (14.8%) and delamination (9%).

5. The damage behavior of the composite target indicated interply delamination, fiber and matrix failure as the possible modes of material damage under ballistic impact. The fiber tensile damage is the predominant failure mechanism, followed by the mode of fiber damage due to compressive loading and the matrix shear failure mechanism is comparatively insignificant.

6. Cohesive interface parameters, i.e. interface stiffness (K_i), interface strength (t_i^{max}) and critical energy release rate (G_i^C) have significant effects on the overall target behavior, on the amount of dissipated energy due to interply delamination and on the impact induced delamination pattern in composites. More specifically, the interply shear properties of the cohesive interface found play an important role in controlling the energy dissipated by delamination. The higher the interply shear properties are, the higher the dissipation by delamination is. Adversely, ballistic resistance is almost insensitive to the increase in the interface properties in normal failure mode. When the shear adhesive parameters $t_{s,t}^{max}$, $G_{s,t}^C$ increased by 100%, the residual velocity decreased by approximately 5.7% and the amount energy dissipated due to delamination increased by approximately 22.9%.

7. From the damage morphology associated with interface parameters, it was found that the predicted damage evolution parameter was positively correlated to the delamination interface properties. At low values of t_i^{max} and G_i^C (−50%), the largest delamination damaged areas appear while at high values of interface parameters (+50%), the delamination areas were confined to a small area localized around the perforated hole.

8. Stacking sequence of the plies has considerable influence on the failure pattern and energy absorption of the composite target under ballistic impact. At impact velocity of 300 m/s, the configuration $[0/90]_{4s}$ was found to have the highest drop in residual velocity (165 m/s) compared to others and thus the higher increase in internal energy (233.5 J).

9. The support condition of the target plays insignificant effect on the ballistic performance of the laminated target. In general, the energy absorbing capacity of the target laminate increases slightly as the boundary condition of the target released from C-C to C-F or S-S. The differences in residual velocity, due to the change in the boundary state from C-C to C-F and C-C to S-S, were found to decrease by 1 m/s and 0.8 m/s, respectively.

10. Conclusively, the results from this study could help the authors in future work in designing laminated composite targets with better ballistic resistance through selecting parameters to vary in order to achieve better impact performance against high perforation velocities, and thus help in reducing the experimental effort associated with their design.

Declaration of competing interest

The authors declare that they have no known competing financial interests or personal relationships that could have appeared to influence the work reported in this paper.
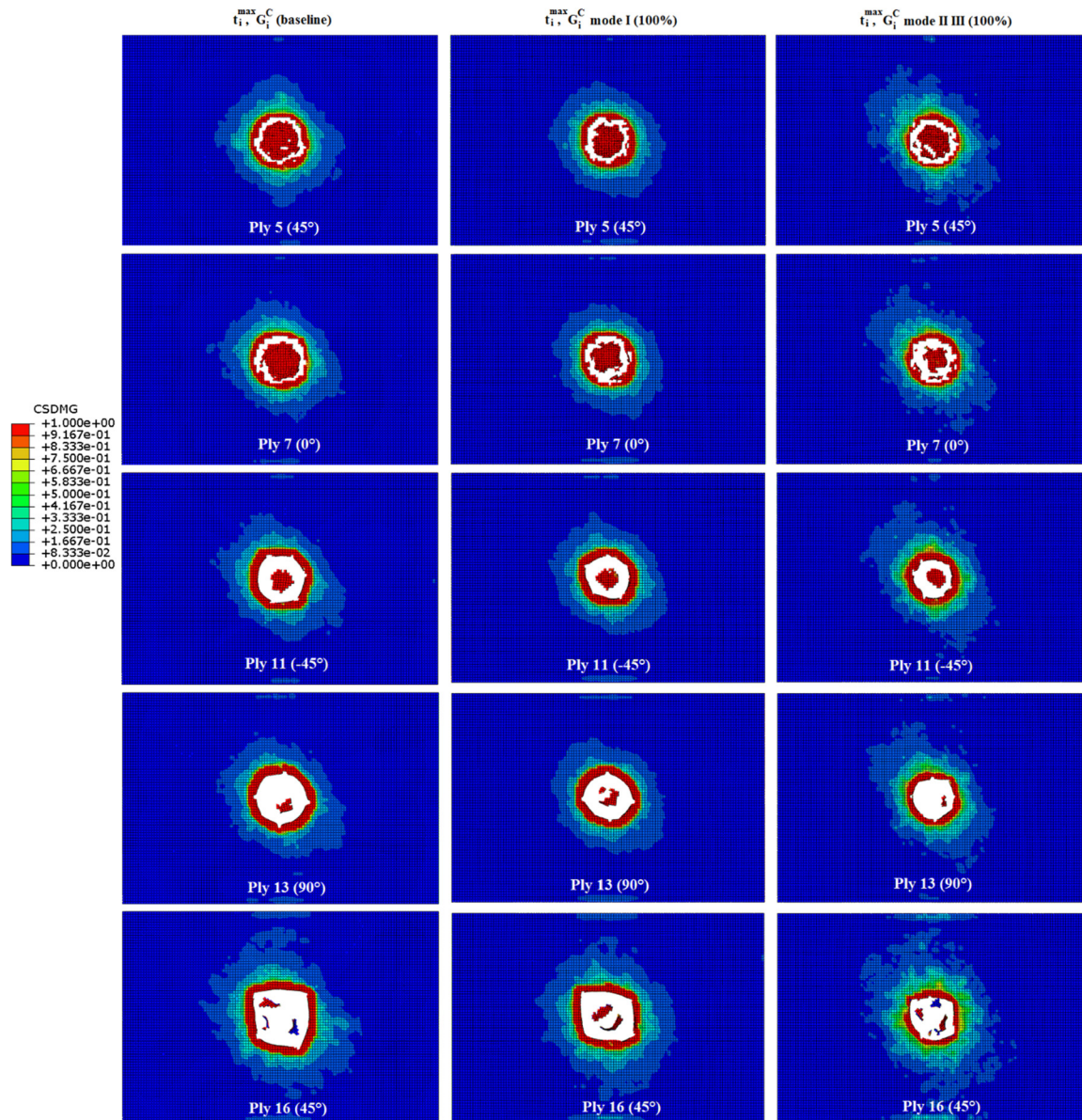
Fig. 22. Degree of delamination growth influenced by delamination interface properties in shear (Mode II, III) and tensile (Mode I).

References

[1] A. Viglietti, E. Zappino, E. Carrera, Free vibration analysis of variable angle-tow composite wing structures, Aerosp. Sci. Technol. 92 (2019) 114–125.

[2] S.J. Park, M.K. Seo, Carbon fiber-reinforced polymer composites: preparation, properties, and applications, in: Polymer Composites, vol. 1, Wiley-VCH Verlag GmbH & Co. KGaA, Weinheim, Germany, 2012.

[3] B.R. Thakur, S. Verma, B.N. Singh, D.K. Maiti, Dynamic analysis of folded laminated composite plate using nonpolynomial shear deformation theory, Aerosp. Sci. Technol. 106 (2020) 106083.

[4] S. Abrate, Impact on Composite Structures, 1st ed., Cambridge University Press, 1998.

[5] X.-Y. Zhou, P.D. Gosling, Z. Ullah, L. Kaczmarczyk, C.J. Pearce, Stochastic multi-scale finite element based reliability analysis for laminated composite structures, Appl. Math. Model. 45 (2017) 457–473.

[6] L. Lia, L. Sun, T. Wang, N. Kang, W. Cao, Repeated low velocity impact response and damage mechanism of glass fiber aluminium laminates, Aerosp. Sci. Technol. 84 (2019) 995–1010.

[7] Y. Zhou, Y. Sun, T. Huang, W. Cai, SPH-FEM simulation of impacted composite laminates with different layups, Aerosp. Sci. Technol. 95 (2019) 105469.

[8] S.N.A. Safri, M.T.H. Sultan, M. Jawaid, K. Jayakrishna, Impact behaviour of hybrid composites for structural applications: a review, Composites, Part B, Eng. 133 (2018) 112–121.

[9] X. Li, D. Ma, H. Liu, W. Tan, X. Gong, C. Zhang, Y. Li, Assessment of failure criteria and damage evolution methods for composite laminates under low-velocity impact, Compos. Struct. 207 (2019) 727–739.

[10] B. Kazemianfar, M. Esmaeeli, M.R. Nami, Response of 3D woven composites under low velocity impact with different impactor geometries, Aerosp. Sci. Technol. 102 (2020) 105849.

[11] W. Tan, B.G. Falzon, L.N. Chiu, M. Price, Predicting low velocity impact damage and compression-after-impact (CAI) behaviour of composite laminates, Composites, Part A, Appl. Sci. Manuf. 71 (2015) 212–226.

[12] A. Kursun, M. Senel, Investigation of the effect of low-velocity impact on composite plates with preloading, Exp. Tech. 37 (6) (2013) 41–48.

[13] N. Hongkarnjanakul, C. Bouvet, S. Rivallant, Validation of low velocity impact modelling on different stacking sequences of CFRP laminates and influence of fibre failure, Compos. Struct. 106 (12) (2013) 549–559.

[14] C. Lopes, O. Seresta, Y. Coquet, Z. Gurdal, P. Camanho, B. Thuis, Low-velocity impact damage on dispersed stacking sequence laminates. Part I: experiments, J. Compos. Sci. Technol. 6 (2009) 926–936.

[15] V. Tita, J. Carvalho, D. Vandepitte, Failure analysis of low velocity impact on thin composite laminates: experimental and numerical approaches, Steel Compos. Struct. 8 (2008) 413–428.

[16] Y. Zhang, P. Zhu, X. Lai, Finite element analysis of low-velocity impact damage in composite laminated plates, Mater. Des. 27 (6) (2006) 513–519.

[17] L. Iannucci, Progressive failure modelling of woven carbon composite under impact, Int. J. Impact Eng. 32 (6) (2006) 1013–1043.

[18] T. Mitrevski, I.H. Marshall, R.S. Thomson, R. Jones, Low-velocity impacts on preloaded GFRP specimens with various impactor shapes, Compos. Struct. 76 (3) (2006) 209–217.

[19] M.F.S.F. de Moura, J.P.M. Goncalves, Modelling the interaction between matrix cracking and delamination in carbon-epoxy laminates under low-velocity impact, Compos. Sci. Technol. 64 (7/8) (2004) 1021–1027.

[20] J. Lua, W. Gregory, Development of a dynamic failure prediction tool for marine composite structure, J. Appl. Mech. 256 (7) (2005) 299–308.

[21] Y.J. Lee, C.H. Huang, Ultimate strength and failure process of composite laminated plates subjected to low-velocity impact, J. Reinf. Plast. Compos. 22 (12) (2003) 1059–1081.

[22] G. Schoeppner, S. Abrate, Delamination threshold loads for low velocity impact on composite laminates, Composites, Part A 31 (2000) 903–915.

[23] Z. Guan, C. Yang, Low-velocity impact and impact process of composite laminates, J. Compos. Mater. 36 (7) (2002) 851–871.

[24] R.K. Luo, E.R. Green, C.J. Morrison, An approach to evaluate the impact damage initiation and propagation in composite plates, Composites, Part B 32 (6) (2001) 513–520.

[25] A.F. Johnson, A.K. Pickett, P. Rozycki, Computational method for predicting impact damage in composite structures, Compos. Sci. Technol. 61 (15) (2001) 2183–2192.

[26] K.V. Williams, R. Vaziri, Application of a damage mechanics model for predicting the impact response of composite materials, Comput. Struct. 79 (10) (2001) 997–1011.

[27] J.P. Hou, N. Petrinic, C. Ruiz, S.R. Hallett, Prediction of impact damage in composite plates, Compos. Sci. Technol. 60 (2) (2000) 273–281.

[28] M. Schwab, M. Todt, J. Tauchner, D. Schlie, H.E. Pettermann, Modeling, simulation, and experiments of high velocity impact on laminated composites, Compos. Struct. 205 (2018) 42–48.

[29] J. Pernas-Sánchez, J. Artero-Guerrero, J.Z. Viñuela, D. Varas, J. López-Puente, Numerical analysis of high velocity impacts on unidirectional laminates, Compos. Struct. 107 (2014) 629–634.

[30] J. López-Puente, R. Zaera, C. Navarro, An analytical model for high velocity impacts on thin CFRPs woven laminated plates, Int. J. Solids Struct. 44 (9) (2007) 2837–2851.

[31] M. Yamada, Y. Tanabe, A. Yoshimura, T. Ogasawara, Three-dimensional measurement of CFRP deformation during high-speed impact loading, Nucl. Instrum. Methods Phys. Res., Sect. A, Accel. Spectrom. Detect. Assoc. Equip. 646 (1) (2011) 219–226.

[32] R. Higuchi, T. Okabe, A. Yoshimura, T.E. Tay, Progressive failure under high-velocity impact on composite laminates: experiment and phenomenological mesomodeling, Eng. Fract. Mech. 178 (2017) 346–361.

[33] R.A.W. Mines, S. McKown, R.S. Birch, Impact of aircraft rubber tyre fragments on aluminium alloy plates: I-Experimental, Int. J. Impact Eng. 34 (2007) 627–646.

[34] D. Zhang, Q. Fei, Effect of bird geometry and impact orientation in bird striking on a rotary jet-engine fan analysis using SPH method, Aerosp. Sci. Technol. 54 (2016) 320–329.

[35] P. Guégan, R. Othman, D. LeBreton, F. Pasco, N. Swiergiel, P. Thevenet, Experimental investigation of rubber ball impacts on aluminium plates, Int. J. Crashworthiness 15 (4) (2010) 391–399.

[36] Y. Zhou, Y. Sun, T. Huang, Bird-strike resistance of composite laminates with different materials, Materials 13 (1) (2020) 129.

[37] J. Cai, H. Bao, H. Zuo, Y. Huang, Safety evaluation of airworthiness requirement of bird-strike on aeroplane, Eng. Fail. Anal. 102 (2019) 407–416.

[38] N.K. Naik, A.V. Doshi, Ballistic impact behavior of thick composites: analytical formulation, AIAA J. 43 (7) (2005) 1525–1536.

[39] N.K. Naik, P. Shrirao, Composite structures under ballistic impact, Compos. Struct. 66 (2004) 579–590.

[40] H.M. Wen, Predicting the penetration and perforation of FRP laminates struck normally by projectiles with different nose shapes, Compos. Struct. 49 (3) (2000) 321–329.

[41] H.M. Wen, Penetration and perforation of thick FRP laminates, Compos. Sci. Technol. 61 (8) (2001) 1163–1172.

[42] N.K. Naik, P. Shrirao, B.C.K. Reddy, Ballistic impact behaviour of woven fabric composites: formulation, Int. J. Impact Eng. 32 (2006) 1521–1552.

[43] N.K. Naik, J.V. Joshi, Ballistic impact behaviour of thick composites: parametric studies, Compos. Struct. 82 (2008) 447–464.

[44] C.F. Yen, A ballistic material model for continuous-fiber reinforced composites, Int. J. Impact Eng. 46 (2012) 11–22.

[45] P.R.S. Reddy, T.S. Reddy, V. Madhu, A.K. Gogia, K.V. Rao, Behavior of E-glass composite laminates under ballistic impact, Mater. Des. 84 (2015) 79–86.

[46] M. Karahan, A. Jabbar, N. Karahan, Ballistic impact behavior of the aramid and ultra-high molecular weight polyethylene composites, J. Reinf. Plast. Compos. 34 (1) (2015) 37–48.

[47] S. Patel, S. Ahmad, P. Mahajan, Probabilistic failure analysis of composite beams for optimum ply arrangements under ballistic impact, J. Aerosp. Sci. Technol. 1 (2015) 36–47.

[48] W. Tan, B.G. Falzon, L. Chiu, M. Price, Predicting low velocity impact damage and Compression-After-Impact (CAI) behaviour of composite laminates, Composites, Part A 71 (2015) 212–226.

[49] K.S. Pandya, J.R. Pothnis, G. Ravikumar, N.K. Naik, Ballistic impact behavior of hybrid composites, Mater. Des. 44 (2013) 128–135.

[50] L.M. Bresciani, A. Manes, A. Ruggiero, G. Iannitti, M. Giglio, Experimental tests and numerical modelling of ballistic impacts against kevlar 29 plain-woven fabrics with an epoxy matrix: macro-homogeneous and meso-heterogeneous approaches, Composites, Part B 88 (2016) 114–130.

[51] L.M. Bresciani, A. Manes, M. Giglio, An analytical model for ballistic impacts against plain-woven fabrics with a polymeric matrix, Int. J. Impact Eng. 78 (2015) 138–149.

[52] A.K. Bandaru, L. Vetiyatil, S. Ahmad, The effect of hybridization on the ballistic impact behavior of hybrid composite armors, Composites, Part B 76 (2015) 300–319.

[53] M. Ridha, T.E. Tay, S. Werner, P. Joern, V.B.C. Tan, Analysis of composite stiffener under successive impact and bending test, J. Reinf. Plast. Compos. 36 (17) (2017) 1225–1238.

[54] E. González, P. Maimí, P. Turon, J. Mayugo, Simulation of drop-weight impact and compression after impact tests on composite laminates, Compos. Struct. 94 (11) (2012) 3364–3378.

[55] A.F. Johnson, Modelling fabric reinforced composites under impact loads, Composites, Part A 32 (2001) 1–2.

[56] P. Maimí, P.P. Camanho, J.-A. Mayugo, C.G. Dávila, A thermodynamically consistent damage model for advanced composites, Technical Report NASA TM-2006-214282, NASA, 2006.

[57] A.F. Johnson, J. Simon, Modeling fabric reinforced composites under impact loads, in: EUROMECH 400: Impact and Damage Tolerance of Composite Materials and Structures, Imperial College of Science Technology & Medicine, London, 1999.

[58] X.C. Sun, M.R. Wisnom, S.R. Hallett, Interaction of inter-and intralaminar damage in scaled quasi-static indentation tests: Part 2–numerical simulation, Compos. Struct. 13 (2016) 727–742.

[59] S.T. Pinho, P.P. Camanho, M.F. De Moura, Numerical simulation of the crushing process of composite materials, Int. J. Crashworthiness 9 (3) (2004).

[60] M. Schwab, M. Todt, M. Wolfahrt, H.E. Pettermann, Failure mechanism based modelling of impact on fabric reinforced composite laminates based on shell elements, Compos. Sci. Technol. 128 (2016) 131–137.

[61] M.V. Mousavi, H. Khoramishad, The effect of hybridization on high-velocity impact response of carbon fiber-reinforced polymer composites using finite element modeling, Taguchi method and artificial neural network, Aerosp. Sci. Technol. 94 (2019) 105393.